Fuel 406 (2026) 136681

Contents lists available at ScienceDirect

Fuel

journal homepage: www.elsevier.com/locate/fuel

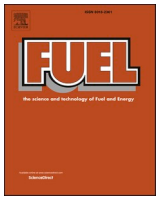

Full Length Article

The composition of gases from a diffusion flame above longleaf pine needle fuel beds

David.R. Weise [a,*], Thomas H. Fletcher [b], Timothy J. Johnson [c], WeiMin Hao [d], Russell G. Tonkyn [c], Catherine A. Banach [c], Javier Palarea-Albaladejo [e], Mahsa Alizadeh [b], Stephen Baker [d]

[a] USDA Forest Service, Pacific Southwest Research Station, Riverside, CA, USA
[b] Brigham Young University, Department of Chemical Engineering, Provo, UT, USA
[c] Pacific Northwest National Laboratory, Richland, WA, USA
[d] USDA Forest Service, Rocky Mountain Research Station, Missoula, MT, USA
[e] University of Girona, Department of Computer Sciences, Applied Mathematics and Statistics, Girona, Spain

ARTICLE INFO

Keywords:
Wildland fire
Flame
Pyrolysis
Biomass
Tars
Fourier transform infrared spectroscopy
Gas chromatography
Compositional data analysis

ABSTRACT

The gas and tar composition of a wildland fire diffusion flame from longleaf pine needles is currently relatively unmeasured and more data are needed to fill in the gap between pyrolysis data and smoke plume data, thus improving physical and chemical modeling of wildland smoke formation. A pilot experiment to measure light gas and tar composition of such a flame is described for three flame zones: persistent flame (flame base), intermittent flame, and smoke plume. Flame gases from 24 experimental fires were collected in canisters and analyzed for CO_2, CO, H_2, CH_4, and C_2 to C_7 hydrocarbon gases. Other light gases were measured using FTIR spectroscopy. Condensed gas (tar) samples were collected and analyzed using GC/MS. Results from compositional data analysis suggest significant differences in (relative) concentration of compounds detected in the three zones. Statistical tests for differences in flame zones were performed using canister data. Concentration of hydrocarbons relative to CO and CO_2 decreased from the persistent flame zone through the intermittent flame zone into the flame-free plume. This was likely due to oxidation reactions in the flame as well as entrainment of air into the flame/plume. Partial agreement between persistent flame zone composition and pyrolysis data for a global kinetic model provided support for future use of the kinetics model in physically-based fire models. The identification of gases and tars in different flame zones supported a conceptual model of a wildland flame.

1. Introduction

The flame of a wildland fire is a buoyant diffusion flame that originates from the pyrolysis of solid plant materials and combustion of the resulting pyrolysis gases in an uncontrolled environment resulting in a significant release of energy and combustion products [1]. Pyrolysis of plant materials yields gases, tars, ash and char [2–4]; the inorganic ash content can affect pyrolysis [5]. Combustion of the pyrolysis products yields gases, tars (which can form particulates), elemental carbon, organic carbon, and inorganic ash [6–8]. Methods to capture the energy produced by combustion of these biofuels for useful purposes has been a pursuit of humans since time immemorial [9]. Early work focused on the use of wood to produce charcoal and increase the energy density in the fuel. Starting with the energy crisis in the 1970 s, biofuels and methods to produce energy efficiently while minimizing noxious combustion products have been studied extensively e.g., [10]. Various processes such as gasification and pyrolysis (with or without O_2) can produce a variety of gas mixtures containing H_2, CO, CO_2, methane, ethane, N_2, formic acid, acetic acid, glyoxal and many other hydrocarbons [11–13] which are then potentially used to produce energy. These processes also can produce "waste" gases which can be captured and used for other purposes. It is generally acknowledged that these biomass processes are more efficient in terms of energy capture and combustion completeness when compared with open burning which is uncontrolled and potentially more variable than the controlled, optimized burning to produce energy.

Reaction mechanisms in the flames produced by the burning of biomass-derived fuel mixtures containing H_2, CO, methane, CO_2, and N_2

* Corresponding author.
E-mail address: david.weise@usda.gov (David.R. Weise).

https://doi.org/10.1016/j.fuel.2025.136681
Received 23 April 2025; Received in revised form 29 August 2025; Accepted 30 August 2025
Available online 23 September 2025

have been studied experimentally and with chemical kinetic simulations [14–16]. As the motivation to burn biomass is energy production, simulations have been constructed to model various combustor setups including stoves. Composition of gases in restricted airflow devices has been studied to understand conditions in enclosures. While these setups involving biomass pyrolysis and combustion contain common elements with open burning, the conditions such as air flow, oxygen level, and heat transfer rates differ which can affect gas and particulate composition and yield. Results from these engineered processes and apparatuses can provide related information, but application to wildland settings is unknown. For example, a series of experiments compared the composition of pyrolysis gases produced with low (thermogravimetric analysis-like) and high (wildland fire) heating rates in fuel rich (no oxygen) and ambient environments and found significant differences [17].

Description of the gas composition in buoyant, turbulent diffusion flames resulting from open burning has received less study than the physical aspects of these flames [18,19]. Multiple literature searches found very few pertinent articles describing the composition in such a flame (gas and particle). This contrasts with the wealth of information on chemical characterization of gases and particulate matter within the smoke plume. Wildland fire smoke is important because of its effects ranging from the composition of and processes in the atmosphere to effects on human lungs [20–22].

As a result of the importance and risk of wildland fire to humanity, pyrolysis and ignition of wood has been extensively studied; the product composition is known to be affected by temperature and heating rate. Less studied are the pyrolysis and ignition of vegetation foliage (fine fuel) which is typically the first fuel to ignite in a wildland fire [23]. Like wood cells, foliage cells consist of cellulose, hemicellulose and lignin [24]. Foliage typically has less lignin than wood [12,25] while the amounts of cellulose and hemicellulose are comparable. Foliage also includes other components such as sugars, starch, protein, pectins, phenols, and lipids [26].

Pyrolysis products of wood and foliage have been determined from samples containing all these components or from cellulose, hemicelluloses and lignin separately. It is well-established that temperature and heating rate influence the composition of pyrolysis products. In the review by Collard and Blin [27], the similarities and differences in pyrolysis products for the components are shown graphically. For cellulose, pyrolysis below 300 °C produces H_2O, CO_2, CO and char, between 300 and 500 °C levoglucosan ($C_6H_{10}O_5$), furfural and tars are produced and above 500 °C, a mixture of low molecular weight gas and volatile products including H_2 can be produced. For hemicelluloses, pyrolysis products are similar to cellulose's with the addition of formic (HCOOH) and acetic (CH_3COOH) acids. At 400 °C, pyrolysis of lignin and wood produced H_2O, CO_2, CO, low weight hydrocarbons and phenols [27–29]. Collard and Blin [27] indicate that the product yields from the individual components do not necessarily sum to the yield from a lignocellulosic fuel for a variety of reasons.

As vegetation begins to thermally decompose due to a flame, it releases pyrolysis gases into the interior of a flame envelope. Pyrolysis gases diffuse to the flame edge, mix and react with the air, releasing heat. Gases with a variety of molecular weights are released from the surface. The larger molecular weight species that would condense if cooled to room temperature are referred to as tar, whereas the lower molecular weight species that are non-condensable at room temperature are referred to as light gases. Primary pyrolysis is the release of light gas and tars. If the temperatures continue to increase, primary pyrolysis products will continue to react even in the absence of O_2, and this subsequent reaction is referred to as secondary pyrolysis [29–33].

Tars may crack into lighter gases or may polymerize into higher molecular weight polycyclic aromatic hydrocarbons (PAH) leading to soot formation. Some of the light gases may also react to form PAH and eventually soot [34]. The hot, glowing soot particles produce the characteristic yellow color of the visible flame and radiate heat away from the flame to the surroundings. While the pyrolysis gases and soot react with O_2 at the edge of the flame, some of the soot and other hydrocarbons escape the flame zone to form smoke emissions which have been measured and described extensively for over 50 years e.g., [35–37]. Emissions have been measured and described; the various pathways by which a solid wildland fuel pyrolyzes to produce a suite of gases and char which may or may not react to form a flame have not yet been described or modeled.

Prescribed burning is the use of fire under defined fuel and weather conditions to accomplish specific wildland resource management objectives. Because prescribed burning results in a planned release of smoke into the atmosphere, the U.S. Clean Air Act [38] requires estimates of the amount and composition of smoke to be produced. Current estimation methods use the mathematical product of the amount of fuel burned and an emission factor [39]. Understanding what occurs within the flame to produce smoke emissions and the resulting emission factors is needed to improve models and tools.

The interior compositions of laminar diffusion flames from relatively simple gaseous and liquid fuels have been studied carefully e.g., [40,41]. However, the composition of the interior of buoyant turbulent flames from solid vegetative fuels in wildland fires, i.e. the space between the pyrolyzing fuel at the solid surface and the smoke plume, is relatively undescribed [42]. While theoretical constructs of a wildland flame that include thermochemical aspects have been developed [43,44], to our knowledge, measurement of the composition of a wildland flame, i.e., the chemical compounds present in various parts of the flame and their concentrations, has seldom been done.

Most studies of diffusion flames have used devices such as burners which create flames from very simple gas mixtures e.g., [45]. In natural gas flames (principally methane, CH_4) there is little oxygen (O_2) at the base of the flame. The O_2 concentration decreases through the flame edge with little or no O_2 in the interior zone of the flame. There may be some penetration of O_2 gas into the interior of the flame near the flame tip. The composition of the pyrolysis gases from biomass and wildland fuels is far more complex than a simple gas flame especially in regards to the tar compounds [e.g., [46–48]. The buoyant turbulence in a wildland fire and entrainment add complexity due to the turbulent eddies which mix fuel and O_2 and introduce additional O_2 [49].

In a buoyant turbulent diffusion flame, three zones have been previously identified for both circular and line fires: i) the continuous flame, ii) an intermittent zone with pulsating flame, and iii) the plume zone which is generally flame free [1,50]. The composition of exhaust flame gases measured in devices such as the cone calorimeter and the FM Global Fire Propagation Apparatus has usually been restricted to CO, CO_2, and O_2 [51,52] and used to ascertain overall heat release. While the continuous flame has been described as "persistent", measurements of CO, CO_2, O_2 and temperature at the base of a kerosene pool fire suggested that the base had an intermittent character [53]. Except for a study [54] where six gases were identified in a flame spreading along a branch of Siberian pine (*Pinus sibirica* Du Tour), a review of the literature did not find where similar measurements had been made for diffusion flames originating from solid wildland fuels.

While wood pyrolysis has been studied extensively [1], recent work focused specifically on the foliage of vegetation [17]. Laboratory pyrolysis was performed at different heating rates (0.5 to 190 °C/s) and temperatures (500 °C to 800 °C) with a focus on early pyrolysis products. The temperatures and higher heating rates were like conditions found in wildland fires [55]. The light gas yields (dry, ash-free basis) for a given heating rate and temperature did not vary much with plant species. The major light gas species (wt% of dry light gas basis) were CO, followed by CO_2, methane (CH_4), and some H_2. The tar species varied quite a bit between plant species. If the primary tar was collected at a low enough temperature (500 °C), the tar species were generally aliphatic compounds plus one-ring aromatics with hydroxyl (–OH) and methoxy ($–OCH_3$) moieties. If the pyrolysis gases were collected in a higher gas temperature environment (750 to 800 °C), aromatic species with 2 to 5 rings were observed, and the substituted species were largely

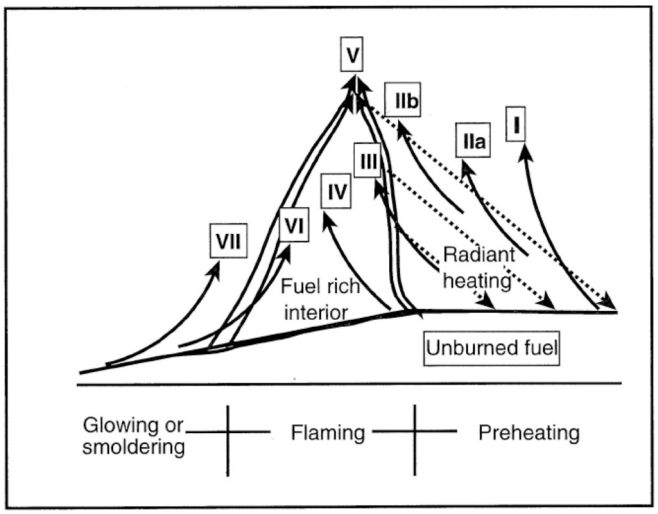

Fig. 1. Conceptual model for a wildland fire diffusion flame [6]. Reprinted from "Forest Fires", D. Ward, Chapter 3 Combustion Chemistry and Smoke, p. 61, Copyright (2001), with permission from Elsevier.

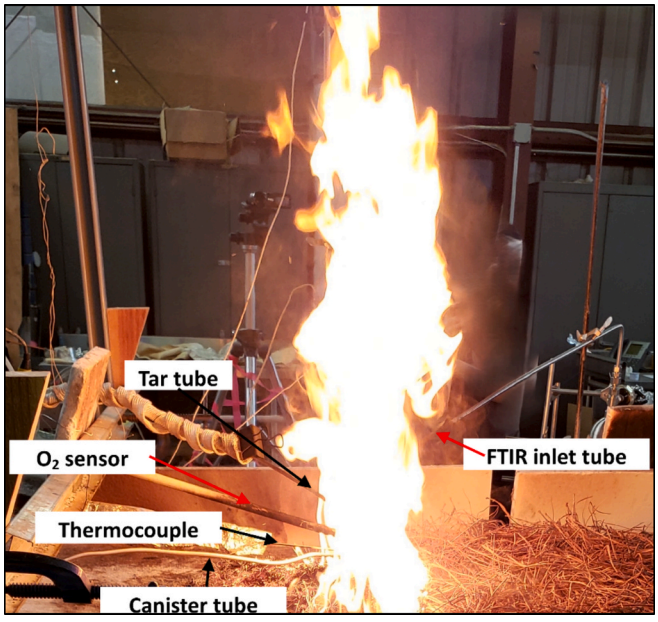

Fig. 2. Moving fuel bed on conveyor belt to keep flame at a fixed point to measure flame gas composition in three zones of a wildland fire flame. Unburnt fuel moves into flame from right side. Approximate locations for gas canister, FTIR spectrometer, tar and temperature samples shown. Setup inspired by other fuel bed conveyor systems [68,69].

not present save for some phenol [46,56,57]. A reanalysis of these results using the compositional data analysis approach confirmed many of these findings [58]. Tar was shown to contain approximately 85 % of the heat of combustion [59]. Related work performed extensive chemical analysis of the same plant species and examined the relationship between the chemical constituents with specific heat capacity [26,60].

Conceptual models such as Fig. 1 suggest the composition of the interior of a flame; however, there is a paucity of data confirming these models. The heat of combustion changes with location within the flame due to the change in gas and tar species as well. This paper presents measurements of gas and tar composition made in a buoyant diffusion flame produced by the burning of a homogeneous fuel bed composed of a single wildland fuel type to determine if the interior gas composition of the flame differs between different zones. While a wildland flame includes particles, which produce its characteristic yellow color, the necessary equipment to characterize particles in the present study was not available at the time of the study (two weeks before the COVID pandemic shutdown in the United States). Agreement with (or support for) the conceptual model was examined.

2. Material and methods

2.1. Experimental and analytical

As this was an initial look at flame composition, a simplified flame setup was used. Burning uniform fuel beds of wildland fuels in a laboratory under controlled conditions is a well-established approach used to study wildland fire characteristics [61–63]. Linking results from laboratory experiments to field conditions can be challenging and has been done to verify results or adjust laboratory results [64–66]. The heating rate of fuels in the laboratory was confirmed to be similar to the heating rate in prescribed fires [65]. The experiments reported here used a common wildland fuel with no imposed wind, and ignited the fuels to simulate a spreading line fire as would be done in a prescribed burn. The fuel moisture content was allowed to equilibrate to ambient atmospheric conditions; as a result, the fire behavior was like what would occur under similar field conditions, i.e. a low intensity surface fire.

Fuel beds of longleaf pine (*Pinus palustris* Mill.) needles from the southern United States (The Pine Straw Store, Augusta, GA, USA)[1] were placed on a conveyor belt apparatus and ignited (Fig. 2). A mass of 1.2 kg wet weight of dead pine needles was evenly distributed (0.5 m × 1.6 m × 0.1 m (W × L × D)) to yield a wet fuel loading of 1.5 kg m^{-2} [67]. Ambient temperature ranged from 25 to 30 °C and building relative humidity ranged from 10 to 18 percent. The pine needle fuel moisture content ranged from 7 to 10 percent dry weight basis. The elemental composition (dry ash-free (daf) wt%) of the pine needles determined by ultimate analysis was C (52.31), H (6.09), N (2.31), S (0.06) and O (39.23). Proximate analysis yielded ash (1.77 wt%), volatile material (78.3 daf wt%) and fixed C (21.7 daf wt%) percent [46]. As seen in Fig. 2, the conveyor belt moved the fuel bed to maintain the flame at a constant position relative to the sampling probes [68,69]. Twenty-four experiments were performed.

Sample probes were located along a vertical slice along the centerline of the flame immediately above the pyrolyzing fuel (persistent flame), in the intermittent flame zone and in the buoyant plume, bottom to top, respectively. The persistent flame zone roughly corresponds with Ward's zones III, IV and VI while the intermittent zone corresponds with Ward's III and V zones (Fig. 1). Gas temperatures were sampled in each zone at 1 Hz using type K (chromel–alumel) 0.25 mm bare wire thermocouples. It is well-established that temperature of a thermocouple is the bead temperature, not the gas temperature in a fire environment [70,71]. Measured temperatures were adjusted for radiation loss from the bead to estimate the gas temperature [72]. These measurements were designed simply to provide a gross estimate of the temperature of the gas environment in each zone.

For GC analysis gases were collected via a steel tube into an evacuated canister. Analysis of the canister gases was performed at the Forest Service's Missoula Fire Sciences Laboratory in Montana. All canisters were analyzed using EPA method TO-14A [73] for CO_2, CO, CH_4, and C_2 to C_7 hydrocarbon gases with an Agilent model 7890 gas chromatograph configured with two columns running simultaneously. A 3.175 mm diameter, 2 m Carbosphere packed column with a nickel catalyst methanizer was used for analysis of CO_2 and CO using a flame ionization detector (FID) [74]. The second column, a 0.53 mm diameter x 50 m

[1] The use of trade or firm names in this publication is for reader information and does not imply endorsement by the U.S. Department of Agriculture of any product or service.

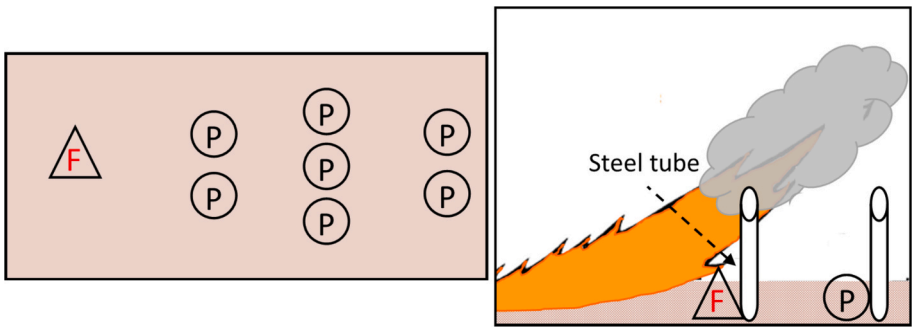

Fig. 3. Wind tunnel canister gas-sampling system used to sample pre-flame 'P' and flaming 'F' combustion gas samples, respectively. Planform view (left) shows approximate location of sample tubes in longleaf pine needle fuel bed. Side view (right) shows location of pyrolysis sampling tubes relative to flame and smoke plume.
Adapted from Figure 1 in [65].

length Agilent Al/S column, separated hydrocarbons and methane. Both columns were analyzed by FID detectors and were run simultaneously. Chromatogram data were collected and processed by Agilent OpenLab software. For measurement of hydrogen gas, a Trace Analytical RGA3 reduction gas analyzer was used. This is a chromatographic instrument with a molecular sieve column, N_2 carrier gas, and a UV mercuric oxide detector that provides sensitive, precise measurement of H_2. The measurement range is 0—20 ppm H_2. Most samples were above this concentration and were diluted with UHP nitrogen prior to analysis. A 10 ppm hydrogen standard (Scott Specialty Gases) was used for calibration.

Gases were also collected by a single probe connected via 3/8 inch heated metal tubing (70 °C) to a Bruker Tensor 37 (T37) spectrometer/gas cell system in static mode. The White cell was held at approximately 55 °C to keep the gases and particulates from condensing inside the cell. The cell was coupled to a purged FTIR spectrometer (Bruker Tensor 37) equipped with a glow bar source, germanium on potassium bromide (Ge/KBr) beamsplitter, and liquid-nitrogen-cooled (N_2) mercury cadmium telluride detector. Spectra were collected from 4000 to 500 cm^{-1} at 0.6 cm^{-1} resolution [75–78]. Spectral analysis was carried out using the MALT5 program [79] and 50 °C reference spectra from the PNNL database [80,81] as well as absorption lines from HITRAN [82]. MALT5 fitted the assigned reference spectral lines to the measured spectrum by optimizing the fit of all gases ascribed to the spectral window and minimizing the residual. The calculation involved input parameters such as path length, resolution, and apodization function, accompanied by reference absorption cross sections and the measured spectrum with its associated temperature–pressure values. Both H_2O and CO_2 had lines that were saturated; these zones were eliminated from analysis. In some instances, absorption peaks for the gases of interest were also saturated, in which case the pressure in the gas cell was reduced and the measurement repeated. The goal of the static mode was to obtain a higher resolution, higher fidelity spectral "snapshot" for a given point in time of the burn; more interferograms were averaged at higher spectral resolution thus allowing for detection of more gaseous species with higher sensitivity.

The amount of O_2 was measured with an Econox CarboProbe^{TM} HT near the other sample lines (Fig. 2). The sensor required an operating temperature of 600 °C and calculated the percent of O_2 based on a millivolt output linked to absolute temperature and two O_2 partial pressures (in the flame gas mixture and in the pure reference air) using the Nernst equation [83,84]. The sensor was heated above 200 °C with a flat plate burner prior to each experiment to reduce equilibration time. The sensor is unheated, and its actual operating temperature (measured with a thermocouple) was determined by the temperature of the immediate flame environment. Reference air was not introduced into the flame leaving the local O_2 concentration unaffected. Any local oxidation reactions occurring in the vicinity of the sensor were a result of the flame environment, not the sensor.

Tar samples were collected by pumping gaseous products from the flame zone through heated (300 °C) 1/4 inch stainless steel tubing into glass tubes containing glass wool in an ice bath in a manner similar to previous work in a flat-flame burner (FFB) environment [46,59]. The test tubes were immediately sealed after the experiment with parafilm for offline analysis. Tars were extracted from the glass wool and the sides of the test tubes using dichloromethane (CH_2Cl_2) as a solvent. Approximately 2 g of anhydrous calcium sulfate ($CaSO_4$) were added to the CH_2Cl_2-tar solution to absorb any H_2O present. To analyze the tar, 1.0 μL of the CH_2Cl_2–tar mixture was injected into a 1310 ThermoFisher gas chromatography mass spectrometer (GC/MS) system equipped with a Restek Rxi-1 ms capillary column (60 m × 0.25 mm × 1 μm). The temperature of the injected sample was held at 50 °C for 5 min, then the temperature was increased to 250 °C at 10 °C/min, and finally held at 250 °C for 5 min. Ultra-high purity (UHP) helium was the carrier gas used in the GC/MS system. Tar compounds were identified by comparing their mass spectra with spectra from the NIST Standard Reference Database 1A [85]. Further analysis of tar samples showed that many tar compounds had low concentrations below the detection limit

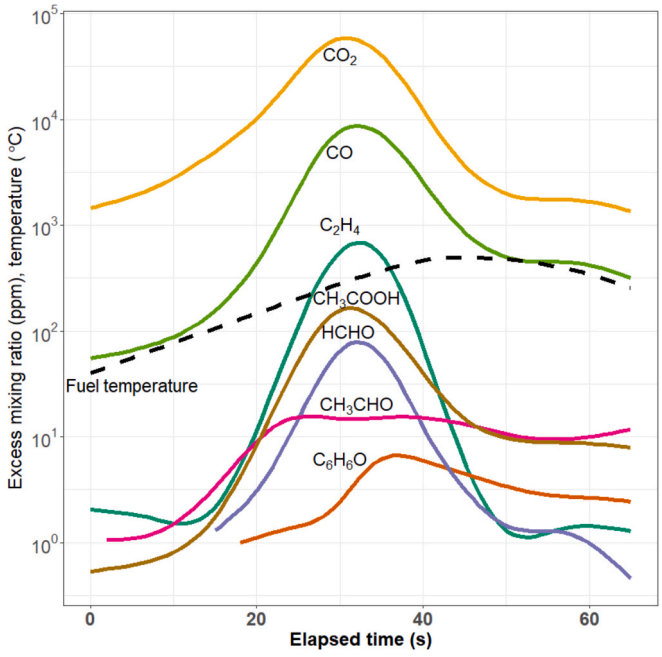

Fig. 4. Smoothed evolution of gas concentrations determined by FTIR spectroscopy in a spreading fire in a longleaf pine fuel bed in a wind tunnel with no wind. Data from [78]. Dashed line is fuel bed temperature below sample probe measured by infrared thermal camera.

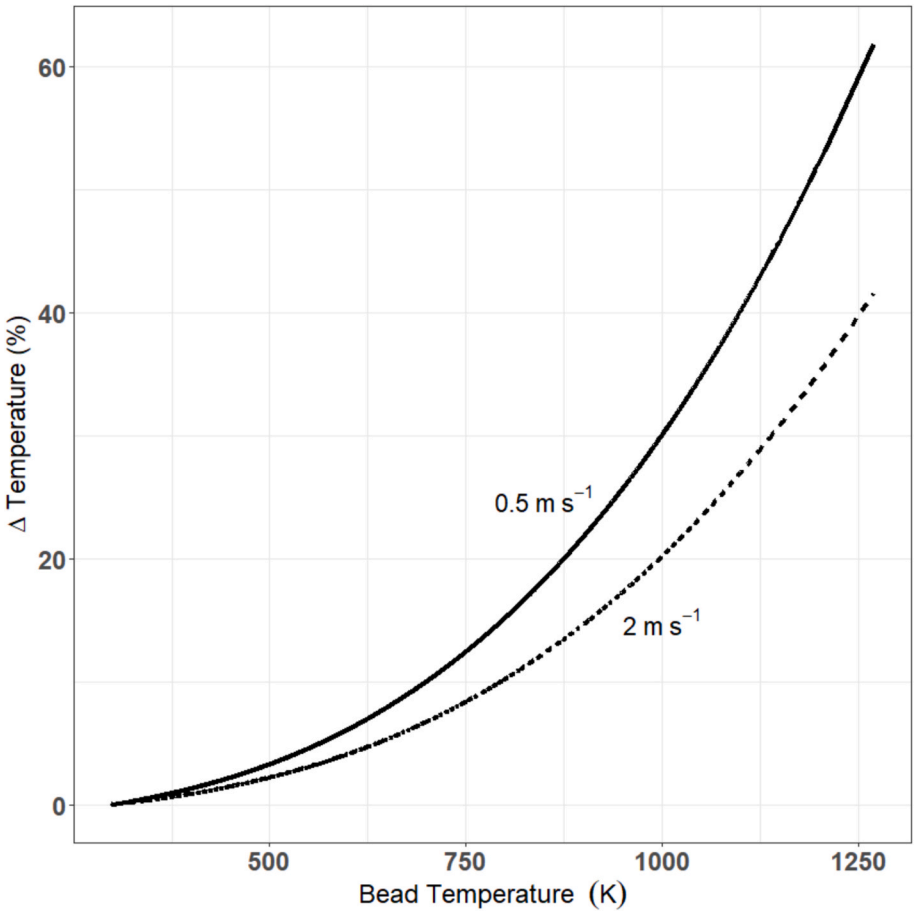

Fig. 5. Difference between calculated flame gas temperature [72] and Type K 0.25 mm thermocouple bead temperature. ΔTemperature = absolute difference between bead and gas temperatures as a percentage of bead temperature.

of the instrument. This made identification of some of tar compounds more difficult. The reported mole fraction for each identified compound is the ratio of the area under the peak associated with that compound to the sum of areas under all detectable and identifiable peaks.

In addition to the 24 pine needle fire experiments on the conveyor belt, pyrolysis gas data from a series of wind tunnel fires were included in the present study [65]. These data represent some of the first measurements of pyrolysis gases in a fire environment under wildland fire conditions (intact fuels, ambient atmosphere). The gases were collected in advance of the flame and represent pyrolysis gases released outside of the flame envelope as the fuel was heating before the moving fire arrived (Fig. 3). Fourteen fire experiments were performed in 2.4 × 0.8 m stationary longleaf pine needle fuel beds; gases were collected in canisters using an array of sample tubes. Moisture content of the needles ranged from 10 to 16 percent dry weight basis and wet fuel loading was 0.52 kg m^{-2}. With similar fuel loading and moisture content, the flame lengths and heat release rates were of the same order of magnitude. Gas quantities were determined using the same analytical chemistry techniques as the canister gases in the present study. The pyrolysis gas sampling locations for these wind tunnel data correspond to Ward's I, IIa and IIb zones (Fig. 1). For all gases, gas quantities were adjusted by subtracting background atmospheric levels and are thus excess values, except for O_2. *Trans*-2-pentene and *cis*-2-pentene amounts were added together as 2-pentene. The samples from these 14 fires represent pre-flame gases including the early stages of pyrolysis. The mass loss of the pine needles was not measured; however, infrared temperatures of the pine needles increased from ambient temperatures to 100 °C in about 120 s and then to maximum temperatures > 400 °C in 10 to 15 s indicating flame arrival. Since the sampling protocol involved manually opening and shutting the sampling tubes and the goal was to not sample flame gases, the mass loss due to pyrolysis that occurred before a sample inlet was shut was probably less than 20 % of the total mass loss. In a mass over time plot (Fig. E-2 in Safdari [86]), a normalized mass decrease of twenty percent in one second in longleaf pine needles heated by convection and radiation in a flat-flame burner (FFB) study described below was reported. In the wind tunnel experiments, which included small plants in the fuel bed, dynamic sampling [78] using the FTIR illustrated the rapidity of the evolution of gas concentration as the flame approached and passed the FTIR sample probe which reflected the mass loss rate (Fig. 4). Using unpublished data for a single plant in the wind tunnel experiment,[2] assuming a mass loss rate of 0.2 g s^{-1} per plant, 5–10 plants immediately adjacent to the FTIR probe and a total mass loss of 7 g per plant, the live plants in the fuel bed would have lost 1 to 2 g per second (three percent) and 7 to 14 g (twenty percent) in seven seconds. This difference in mass changes over time between dead pine needles and live plants is well documented. Further details of the wind tunnel experiments can be found elsewhere [65].

Similarly, tar data collected during fast pyrolysis (heating rates were 4, 180 and 195 °C s^{-1} for radiant only, convective only and radiant with convective modes) of dead longleaf pine needles in a flat flame burner (FFB) [46] were also included (7 observations). To provide pyrolysis conditions and an oxygen-free environment (no combustion), the FFB was operated in a fuel-rich mode (equivalence ratio: $\Phi = 1.13$). The fuel

[2] A. Aminfar, M. Princevac. 2019. Experimental Measurements of Convective Heat Flux Ahead of Fire. 96p. Final report for agreement PSW-16-JV-11272167–026, University of California, Riverside on file.

Table 1
Summary of mean and 95 percentile temperatures (Kelvin) for 0.25 mm type K thermocouples (TC) and flame gas (Gas) in three flame zones assuming flame gas velocities of 0.5 and 2.0 m s^{-1}.

	Persistent			Intermittent			Plume		
Quantile	TC[a]	$Gas_{0.5}$[b]	Gas_2[c]	TC	$Gas_{0.5}$	Gas_2	TC	$Gas_{0.5}$	Gas_2
50	725	806	779	679	741	721	578	609	599
95	1051	1419	1298	969	1233	1146	862	1027	973

a.Thermocouple bead temperature.
b.Gas temperature ($G_{0.5}$) calculated following [72]. Air properties at 300 K: velocity = 0.5 m s^{-1}, density = 1.177 kg m^{-3}, thermal conductivity = 0.0261 W m^{-1} K^{-1}, Prandtl = 0.712, viscosity = 1.85E-5 kg m^{-1} s^{-1}, viscosity at 1000 K = 4.18E-5 kg m^{-1} s^{-1} [123], bead diameter = 0.625 mm, emissivity = 0.8.
c.Gas temperature (G_2) calculated as above with velocity = 2.0 m s^{-1}.

Table 2
Summary statistics for excess gas mixing ratios (ppmv) determined from canister samples by flame measurement zone.

Name	VBDL [a]	Persistent		Intermittent		Plume	
Carbon dioxide (CO_2)	0	91,307	76,373–109,161	30,891	24,789–38,495	13,312	9,559–18,540
Carbon monoxide (CO)	0	79,006	59,642–104,656	1,520.2	973.5–2,373.8	326.2	155.7–683.6
Hydrogen (H_2)	0.	12,120	8,167–17,985	137.4	69.5–271.8	14.1	7.9–24.9
Methane (CH_4)	0	10,277	8,653–12,206	114.9	66.9–197.3	15.9	6.7–37.6
Ethene (C_2H_4)	0	5,683.5	4,788.3–6,746.2	43.0	21.5–85.8	3.6	1.2–10.4
Acetylene (C_2H_2)	2	3,739.5	3,111.7–4,494.1	36.4	16.8–78.9	1.7	0.3–8.8
Propene (C_3H_6)	0	1,043.4	865.1–1,258.6	5.1	2.8–9.3	0.69	0.30–1.59
Ethane (C_2H_6)	0	608.8	501.3–739.4	4.0	2.4–6.6	0.65	0.30–1.43
Pentane (C_5H_{12})	7	314.1	261.4–377.4	0.72	0.31–1.66	0.11	0.03–0.44
1,3-butadiene (C_4H_6)	7	202.7	168.4–244.0	1.4	0.7–3.0	0.11	0.02–0.55
Butene (C_4H_8)	5	151.4	121.7–188.3	0.53	0.33–0.85	0.10	0.05–0.22
Allene (C_3H_4)	7	93.6	78.4–111.7	0.68	0.32–1.46	0.08	0.01–0.57
Hexane (C_6H_{14})	11	79.6	66.4–95.4	0.57	0.27–1.19	0.05	0.01–0.41
Isobutene (C_4H_8)	5	75.4	61.0–93.4	0.34	0.21–0.57	0.07	0.03–0.14
Propane (C_3H_8)	0	61.0	48.4–76.9	0.36	0.25–0.52	0.10	0.06–0.16
trans-2-butene (C_4H_8)	7	30.9	24.9–38.3	0.12	0.08–0.20	0.04	0.02–0.08
2-pentene (C_5H_{10})	30	29.4	22.4–38.5	0.14	0.09–0.20	0.10	
Propyne (C_3H_4)	14	27.4	20.0–37.4	0.13	0.04–0.38	0.03	0.02–0.05
cis-2-butene (C_4H_8)	9	22.7	18.4–27.9	0.09	0.06–0.15	0.03	0.01–0.08
Isopentene (C_5H_{10})	14	15.7	11.9–20.6	0.04	0.02–0.06	0.02	0.01–0.05
Isopentane (C_5H_{12})	23	10.4	8.2–13.3	0.10	0.03–0.31	0.07	
1-butyne (C_4H_6)	23	6.2	3.6–10.8	0.07	0.04–0.15	0.07	
Butane (C_4H_{10})	9	5.8	4.0–8.3	0.04	0.03–0.05	0.02	0.01–0.04
1-hexene (C_6H_{12})	23	3.9	3.0–5.1	0.19	0.07–0.52	0.03	0.01–0.07
1-pentyne (C_5H_8)	30	2.7	1.6–4.5	0.09	0.03–0.27		
Isobutane (C_4H_{10})	25	2.6	2.0–3.4	0.02	0.01–0.03	0.02	0.00–0.07
1-pentene (C_5H_{10})	52	0.57	0.39–0.82				

a.Percentage of values below the detection limit of the measuring instrument.
b.The values in the two columns below each flame zone are the geometric mean and the lower and upper limits of the 95 percent confidence interval. Confidence interval not centered on geometric mean because geometric mean and geometric standard deviation are related by multiplication and division.

was a mixture of methane (26.5 L min^{-1}) and hydrogen (16.6 L min^{-1}). Air (258.8 L min^{-1}) was used as an oxidizer. The samples were heated by convective heat transfer from the post-flame products of the burner (CO_2, H_2O, and CO). The tars were collected above the FFB onto glass wool in tubes and then analyzed as described above.

2.2. Statistical data analysis

Smoke and gas data from fires and plumes are multivariate and contain relative information making them compositional data [87]. While a turbulent diffusion flame may not be in chemical equilibrium, the gas data described in 2.1 are of such type [88]. Because wildland fires are buoyant and turbulent, the degree of air penetration into a time-averaged sample makes conventional comparison difficult, and hence statistical techniques from compositional data analysis (CoDA) become helpful. This approach filters out instrumental effects, which mostly determine the absolute values typically reported [89], and focuses on the relative values of one or several compounds to others. Pyrolysis and smoke data are often expressed in relative units such as mole fraction, mass fraction, and concentration (ppm). The relative values can then be expressed as ratios to other gases resulting in emission ratios (with CO or CO_2), fuel-oxidizer ratios (O_2 or air), or emission factors (relative to the amount of fuel burned). The canister, FTIR and tar data sets comprise three subsets (subcompositions) from the complete set of compounds produced by pyrolysis and combustion of the pine needles.

CoDA relies on log-ratio coordinate representations of relative data to use familiar statistical techniques such as linear regression, principal components analysis, and analysis of variance. One key characteristic of the approach is that the relative relationships between the parts of a composition are invariant to changes in units [90]. While the ratios and log-ratios between gases change as the basis (mole, mass, ppm) changes, the variance structure associated with them does not change, so results from statistical analyses based on this do not change. All data analyses in this study were conducted on the R system for statistical computing v4.4.1 (https://www.R-project.org/) [91], including the use of computer algorithms from some specialized packages as detailed below. Conclusions from statistical testing were based on the usual 5 % significance level in all cases.

Table 3
Summary statistics for excess mixing ratio (ppm) of gases determined by FTIR spectroscopy for flame zones.

Name	VBDL[a]	Persistent[b]		Intermittent		Plume	
Water (H_2O)	0	74,865	20,456–273,992	37,402	26,044–53,712	13,437	222.0–> 300,000
Carbon dioxide (CO_2)	0	65,689	16,632–259,449	30,992	8,328–115,335	8,912	37.0–> 300,000
Carbon monoxide (CO)	0	10,784	4,938.5–23,548	833.0	165.2–4,200.3	226.5	69.7–735.8
Methane (CH_4)	56	2,919.3	2,683.8–3,175.4	62.3		14.4	
Propane (C_3H_8)	89	2,248.9					
Ethene (C_2H_4)	11	1,965.8	1,396.6–2,766.9	47.1	6.3–354.2	4.7	0.1–313.2
Acetylene (C_2H_2)	33	818.5	223.2–3,001.2	54.6	10.3–289.4		
Propene (C_3H_6)	11	476.9	72.2–3,150.5	4.0	0.9–17.3	4.9	0.1–439.0
Formaldehyde (HCHO)	44	408.2	96.2–1,732.4	4.9		4.4	
Hydrogen cyanide (HCN)	33	399.2	119.4–1,335.1	19.3	1.0–362.2	6.7	
Acetic acid (CH_3COOH)	11	279.6	1.6–49,175	10.0	3.8–26.3	15.1	0.00–101,607
Ethane (C_2H_6)	44	277.0	112.1–684.4	12.7	0.00–> 300,000		
Acetaldehyde (CH_3CHO)	33	269.1		6.7	0.78–57.8	38.0	10.9–131.7
Methanol (CH_3OH)	0	179.4	66.8–482.0	5.2	1.9–14.4	1.5	0.06–36.8
1,3-butadiene (C_4H_6)	11	145.6	31.9–664.7	3.6	1.6–8.4	6.9	
Glycolaldehyde ($C_2H_4O_2$)	67	100.2	1.2–8595	3.1			
Furfural ($C_5H_4O_2$)	78	81.4	19.4–342.6				
Furan (C_4H_4O)	56	62.4	0.00–> 300,000	4.6	0.00–> 300,000		
Formic acid (HCOOH)	22	47.4	4.5–502.7	2.2	0.31–15.9	1.3	1.2–1.4
Isoprene (C_5H_8)	89	44.6					
Naphthalene ($C_{10}H_8$)	22	44.5	34.8–56.7	1.3	0.01–260.9	0.49	
Allene (C_3H_4)	44	38.5	13.0–114.4	1.7	0.08–36.3		
Nitrous acid (HONO)	33	25.0	0.00–> 300,000	15.4	8.8–26.9	8.2	
Ammonia (NH_3)	67	10.3				0.73	0.00–> 300,000
Methyl nitrite (CH_3ONO)	67	8.1		1.5		1.7	
Nitrous oxide (N_2O)	33	4.3	1.7–10.7	1.5	1.1–2.2	0.65	
Isobutene (C_4H_8)	89			6.6			
Acrolein (C_3H_4O)	89			3.0			
Benzene (C_6H_6)	89			27.3			
Phenol (C_6H_6O)	56			1.8	0.20–15.5	0.78	
Isocyanic acid (HNCO)	78			2.2		3.7	

a.Percentage of values below the detection limit of the measuring instrument.
b.The values in the two columns below each flame zone are the geometric mean and the lower and upper limits of the 95 percent confidence interval. Confidence interval not centered on geometric mean because geometric mean and geometric standard deviation are related by multiplication and division.

The computation of log-ratios becomes problematic when there are zero values in a compositional data set. This can sometimes occur when a particular analyte is "invisible" to an instrument, such as H_2 or Cl_2 to infrared spectrometers [92]. However, when such cases are identified as instances where the gas concentration was below the detection limit (BDL) of the measuring instrument, a sensible zero replacement by imputation with values below the detection threshold, if specified, or the minimum observed concentrations otherwise, is an accepted approach [93,94]. Thus, using the *zCompositions* package in R, the *lrEM* algorithm was applied in this study for the imputation of zeros in the canister data set (as a regular data set with more observations than measured gases), whereas the *lrSVD* algorithm was used for the FTIR and tar data (since here there were fewer observations than measured gases). Note that before this, any gas missing from 80 percent or more of the observations was considered to provide too poor information and was dropped from further analysis.

Each data set (canister, FTIR and tar) consisted of n samples or observations from a composition of D parts (gases) denoted by $\mathbf{x} = [x_1, \cdots, x_D]$. The sample compositions were closed (normalized) to be expressed in proportions by means of the closure operator (Eq. 2.1). Compositional summary measures included the center (mean composition) $\widehat{\boldsymbol{g}}$ and the total, or metric, variance (totvar) as overall measures of central position and dispersion respectively [90] (Eq. 2.2) where $\widehat{\boldsymbol{g}}_j$ are the geometric means per part and var () refers to the ordinary variance measure. To estimate the mean molecular weight by flame zone for each data set, the center was multiplied by a vector of the molecular weights and then summed. This is equivalent to calculating a weighted mean. The molecular weights were determined using the *MolecularWeight* function in the *OrgMassSpecR* R package [95], which uses the NIST Atomic Weights and Isotopic Compositions with Relative Atomic Masses dataset as reference.

$$C(\boldsymbol{x}) = [x_1, \ldots, x_D] / \sum_{1}^{D} x_j \tag{2.1}$$

$$\widehat{\boldsymbol{g}} = C[\widehat{\boldsymbol{g}}_1, \widehat{\boldsymbol{g}}_2, \ldots, \widehat{\boldsymbol{g}}_D]$$
$$\text{totvar} = \frac{1}{2D} \sum_{k,j=1}^{D} \text{var}\left(\ln \frac{x_k}{x_j}\right) \tag{2.2}$$
$$\text{where the } \widehat{\boldsymbol{g}}_j = \left(\prod_{i=1}^{n} x_{ij}\right)^{1/n}, \text{with } j = 1, \ldots, D$$

Multivariate data analysis consisted of principal components analysis (PCA) [96], applied to all three data sets for exploratory purposes, and permutational multivariate analysis of variance (PERMANOVA) [97], used for inferential purposes on the canister data only since it was the most complete data set (58 samples). The FTIR and tar data sets contained a relatively small number of observations (9 samples each) and many values had to be imputed, so statistical testing results were regarded as not trustworthy enough for generalization. However, exploratory PCA on these limited data was useful to obtain some insight and guide future analyses for a recently started project to investigate and model wildland diffusion flame composition in more detail.[3] PCA partitions the total variance in the data set sequentially so that the first principal component accounts for the largest portion of the total variance, the second component accounts for the next largest portion, and so on. In the CoDA context, PCA is usually applied on so-called centered

[3] D.R. Weise, T.J. Johnson, T.L. Myers, A. Zelenyuk, W.M. Hao, D.O. Lignell, B. Shotorban, S. Mahalingam, J. Palarea-Albaladejo, Project RC24-4043: From fuel to smoke: measuring and modeling the chemistry and composition of the prescribed fire flame and near-field plume, 2024. https://www.serdp-estcp.mil.

Table 4
Summary statistics for tars and permanent gases sampled from persistent and intermittent flame zones in longleaf pine needle fuel beds. Sampling method did not capture any tars in the plume zone.

Name	VBDL[a]	Persistent		Intermittent	
Carbon dioxide[b] (ΔCO_2)	0	10.03	8.51–11.82	3.48	2.37–5.11
Carbon monoxide (ΔCO)	0	6.74	5.18–8.78	0.24	0.07–0.83
Hydrogen (ΔH_2)	0	1.27	1.07–1.51	0.01	0.00–1.68
Methane (ΔCH_4)	0	0.94	0.73–1.21	0.02	0.00–0.11
Biphenylene ($C_{12}H_8$)	67	12.74	0.83–195.5		
Fluorene ($C_{13}H_{10}$)	33	10.99	4.47–27.00		
Ethyl *iso*-allocholate ($C_{26}H_{44}O_5$)	0	9.07	4.23–19.45	23.29	6.09–89.13
9,10-Ethanoanthracene, 9,10-dihydro-11,12-diacetyl- ($C_{20}H_{18}O_2$)	78	8.69	0.01–6415		
Phenanthrene ($C_{14}H_{10}$)	22	8.13	0.79–84.2	5.06	4.49–5.69
3-methylphenol (C_7H_8O)	33	6.83	5.38–8.67		
Bicyclo[4.4.1]undeca-1,3,5,7,9-pentaene ($C_{11}H_{10}$)	33	5.15	1.55–17.13		
Caprolactam ($C_6H_{11}ON$)	22	5.13	1.63–16.17	11.79	5.39–25.78
Phenol (C_6H_6O)	44	4.82	2.66–8.75		
Acenaphthylene ($C_{12}H_8$)	44	4.05	0.45–36.47	4.02	0.21–76.88
2-ethenylnaphthalene ($C_{12}H_{10}$)	56	3.58	0.41–30.87		
Catechol ($C_6H_6O_2$)	56	3.50	2.28–5.37		
Biphenyl ($C_{12}H_{10}$)	33	3.49	1.18–10.35		
6-Methylenebicyclo[3.2.0]hept-3-en-2-one (C_8H_8O)	33	3.19	1.75–5.83		
Azulene ($C_{10}H_8$)	89	2.73			
4-ethylphenol ($C_8H_{10}O$)	56	2.30	0.69–7.69		
2,2,4-trimethyl-1H-quinoline ($C_{12}H_{15}N$)	33	2.07	1.31–3.28	10.20	4.52–22.98
1,2-benzothiazole (C_7H_5NS)	22	1.61	0.74–3.49	7.75	0.00–674,379
Propoxur ($C_{11}H_{15}NO_3$)	67	1.22	0.28–5.23		
2-methylphenol (C_7H_8O)	56	0.99	0.24–4.04		
3,4-dimethylphenol ($C_8H_{10}O$)	67	0.79	0.01–49.59		
Cyclopropanebutanoic acid, 2-[[2-[[2-[(2-pentylcyclopropyl)methyl]cyclopropyl]methyl]cyclopropyl]methyl]-, methyl ester ($C_{25}H_{42}O_2$)	78	0.50	0.00–1,414,291		
1-methylideneindene ($C_{10}H_8$)	78	0.46	0.00–9636		
1-heptatriacotanol ($C_{37}H_{76}O$)	44	0.36	0.035–0.36	5.77	0.35–95.05
6,7-epoxypregn-4-ene-9,11,18-triol-3,20-dione, 11,18-diacetate ($C_{25}H_{32}O_8$)	67	0.29	0.14–0.60		
3-ethylphenol ($C_8H_{10}O$)	89	0.24			
Secalciferol ($C_{27}H_{44}O_3$)	56	0.18	0.00–1165	1.99	0.11–37.30
Ingenol ($C_{20}H_{28}O_6$)	78	0.17	0.00–462,802		
1-ethyl-3-methylbenzene (C_9H_{12})	89	0.12			
3-ethyl-5-(2-ethylbutyl)octadecane ($C_{26}H_{54}$)	67			12.55	6.19–25.47
5,9-Dodecadien-2-one, 6,10-dimethyl-, (E,E))- ($C_{14}H_{24}O$)	78			2.39	0.00–15,114
1-(3-methylphenyl) ethanone ($C_9H_{10}O$)	78			5.37	0.00–167,298
2-ethylhexanal ($C_8H_{16}O$)	89			26.77	
2-octadeca-9,12-dienoxyethanol ($C_{20}H_{38}O_2$)	78			4.01	0.20–79.13

a.Percentage of values below the detection limit of the measuring instrument.
b.Values for excess mixing ratios (Δ) for CO_2, CO, H_2, CH_4 from canister samples for fires on which tar samples were collected.
c.The values in the two columns below each flame zone are the geometric mean (mole percent) and the lower and upper limits of the 95 percent confidence interval. Mole percent calculated as ratio of area under peak for a compound and sum of areas for all compounds. Confidence interval not centered on geometric mean because geometric mean and geometric standard deviation are related by multiplication and division.

log-ratio (*clr*) transformed data, with visualization of possible trends using a biplot graphical display [98]. For PERMANOVA, the canister data were represented in so-called isometric log-ratio (*ilr*) coordinates as ordinarily done in CoDA for modelling purposes [90]. PERMANOVA tested the global hypothesis that the gas mixtures did not differ between the flame zones. Pairwise comparison of the gas mixtures between the flame zones was performed using the *pairwise.perm.manova* function in R [99], with the corresponding p-values being adjusted to control for false discovery rate (FDR) in multiple testing using Benjamini and Hochberg's method [100].

$$\widetilde{z}_k = \sqrt{\frac{r_k s_k}{r_k + s_k}} \ln\left[\frac{\left(\prod_{i=1}^{r_k} x_{k_i}^{+}\right)^{1/r_k}}{\left(\prod_{j=1}^{s_k} x_{k_j}^{-}\right)^{1/s_k}}\right], \quad k = 1, \ldots, D-1 \tag{2.3}$$

To determine and facilitate the interpretation of the effect of flame zone on specific groups of gases, a tailored set of *ilr* coordinates was defined by sequential binary partitioning of the observed composition to produce scientifically meaningful contrasts (a.k.a. balances, $\widetilde{z}_k$, Eq. 2.3) between subsets of parts [90] where the log-ratio term of the equation compares the geometric mean of r_k parts in one subset (in the numerator, indicated with + symbol) with the geometric mean of s_k parts in another subset (in the denominator, indicated with − symbol). The preceding multiplicative factor is a normalization factor formally required to ensure comparability of the balances. For the canister data set, these balances were formed between the various classes of gases and then compared between the different flame zones. The non-parametric Kruskal-Wallis rank sum test was used to statistically compare the similarity of all the flame zone median values of each balance. FDR-adjusted pairwise Wilcoxon rank sum tests (using the *pairwise.wilcox.test* function in R) were used to compare all pairwise differences between flame zone median values for each balance.

3. Results and discussion[4]

For the 24 fires, the ambient air temperature was 24.9 to 30.2 °C with relative humidities of 10 to 18 percent. The calculated ambient H_2O content was 2586 to 5650 ppmv. Fuel moisture content of the longleaf pine needles was 7.3 to 10.1 percent. A total of 58 gas canisters, 9 FTIR gas samples, and 9 tar samples were collected from the experimental

[4] The data for gas composition and experimental conditions have been submitted to the Forest Service Research Data Archive for permanent storage. The tar data are embargoed temporarily because they are part of Mahsa Alizadeh's dissertation.

Table 5
Compositional summary statistics for gas mixing ratios determined by GC/FID from canister samples. CO_2, CO, CH_4, H_2 are excess mixing ratios adjusted for atmospheric concentrations.

Name	Center	Variance contribution[a]
Carbon dioxide (CO_2)	8.51E-01	6.3E+01
Carbon monoxide (CO)	1.13E-01	2.9E+01
Hydrogen (H_2)	1.60E-02	6.4E+00
Methane (CH_4)	1.17E-02	7.3E-01
Ethene (C_2H_4)	4.54E-03	2.7E-01
Acetylene (C_2H_2)	2.48E-03	1.6E-01
Propene (C_3H_6)	5.97E-04	6.3E-03
Ethane (C_2H_6)	5.27E-04	2.8E-03
1,3-butadiene (C_4H_6)	1.19E-04	2.0E-04
Butene (C_4H_8)	8.14E-05	1.4E-04
Pentane (C_5H_{12})	7.95E-05	5.0E-04
Propane (C_3H_8)	6.18E-05	7.6E-05
Isobutene (C_4H_8)	4.81E-05	3.2E-05
Allene (C_3H_4)	3.49E-05	4.3E-05
Propyne (C_3H_4)	2.64E-05	3.2E-04
2-pentene (C_5H_{10})	2.43E-05	5.3E-06
trans-2-butene (C_4H_8)	2.15E-05	5.9E-06
Hexane (C_6H_{14})	1.77E-05	3.1E-05
cis-2-butene (C_4H_8)	1.49E-05	2.8E-06
Butane (C_4H_{10})	9.51E-06	5.0E-05
Isopentane (C_5H_{12})	5.99E-06	4.2E-06
Isopentene (C_5H_{10})	4.66E-06	1.7E-06
Isobutane (C_4H_{10})	3.62E-06	3.8E-04
1-hexene (C_6H_{12})	2.71E-06	1.0E-07
1-butyne (C_4H_6)	2.52E-06	4.6E-07
1-pentene (C_5H_{10})	1.66E-06	2.4E-07
1-pentyne (C_5H_8)	1.50E-06	4.6E-06

a.Percentage of variation that the gas contributed to the total variance (totvar), totvar = 0.105.

fires. The chemical and spectroscopic analyses identified 27, 31 and 34 compounds in the canister, FTIR and tar samples, respectively. The ranges of molecular weights (amu) of chemical species detected in the three data sets were 2.016 to 86.18, 16.043 to 128.169 and 94.111 to 536.999, respectively. The measurements and summary statistics are presented in Section 3.1, the PCA and PERMANOVA results in Section 3.2, and the estimated effects of flame zone on selected balances for the canister data are discussed in Section 3.3.

As anticipated, the difference between the thermocouple bead temperature and calculated flame gas temperature increased as temperature increased (Fig. 5). As the assumed vertical velocity of the flame gases increased from 0.5 to 2.0 m s^{-1}, the difference between the gas temperature and the thermocouple temperature decreased. The highest temperatures were observed at the base of the flame and decreased vertically through the flame and plume (see supplemental information). The gas sampling locations were 10, 34, and 58 cm above the fuel bed surface for the persistent, intermittent and plume zones, respectively. Temperature fluctuated appreciably so the 50th (median) and 95th percentile values were computed for all 24 fires for both the thermocouple and gas temperatures (Table 1). Using an assumed gas velocity of 0.5 m s^{-1}, in the persistent zone, median gas temperature ($G_{0.5}$) was approximately 80 K higher than the thermocouple temperature and 360 K higher at the 95th percentile. The 95th percentile gas temperature for the persistent zone was nearly 400 K higher than the plume zone. With an assumed velocity of 2.0 m s^{-1}, the gas temperatures (G_2) were intermediate between the bead temperatures and the 0.5 m s^{-1} gas temperatures.

To determine O_2 concentration, the oxygen sensor must achieve a temperature of 600 °C (873 K). For the 0.5 m s^{-1} gas velocity, the percentile values for 873 K were 55, 65 and 86 for the persistent, intermittent and plume zones, respectively. The percentiles only changed slightly using the higher gas velocity. These percentile values suggest that the necessary sensor temperature was achieved for sufficient time for the persistent and intermittent zones. With this assessment of the reliability of the O_2 sensor, O_2 concentration was 0 percent in all persistent flame zones (11 fires) and 6 of 9 fires for the intermittent flame zone (see supplemental information). The persistent zone corresponds to the fuel rich interior in the conceptual model (Fig. 1). Oxygen was not depleted below atmospheric concentration in the plume zone. In the persistent flame zone, O_2 was depleted up to 100 s or more while the time for depletion in the intermittent zone was much shorter (10 s of seconds). In [54], the amount of O_2 also decreased to near 0 for at least 10 s as the flame base passed by the sample probe. This trend in O_2 concentration is in agreement with the vertical change in relative concentration for O_2 in a typical diffusion flame (Fig. 4 in [6]) which shows no O_2 in the region where pyrolysis occurs with an increase in the region where oxidation reactions occur and then further increase to atmospheric levels above the reaction zone.

3.1. Summary statistics

The center (geometric mean) and 95 percent confidence interval based on the geometric standard deviation [101] for the measured quantities for the canisters, FTIR and tar samples are presented in Table 2, Table 3, and Table 4, respectively, by flame zone. Given the nature of the confidence interval for a geometric mean, many of the confidence intervals overlapped. This observation by itself, however, was not sufficient to state differences between compounds or flame zones. These values do not include the additional wind tunnel or FFB data. The three major gases (CO_2, CO, and CH_4) had the highest observed amounts in all flame zones in the canister and FTIR data while H_2 was the fourth major component in the canister data. The tar data set did not include these gases. The mean amounts of the major gases decreased from the persistent flame to the intermittent flame to the plume. In the canister data set, the percentage of observations with BDL values ranged up to 52.3 percent for 1-pentene. The number of gases observed in only a single sample or not at all was lowest in the persistent flame and greatest in the plume. This could be due to concentrations below detection levels or the gas not being present due to reactions in the flame.

After the BDL values were imputed (replaced with estimated values), and the canister data (58 observations, 27 gases) were closed (Eq. 2.1), CO_2, CO, H_2 and CH_4 still had the highest relative amounts (Table 5). CO_2, CO and H_2 varied considerably between the flame zones and contributed 98.8 percent to the total variance with CO_2 accounting for 63 percent. When plotted by flame zone, the amounts of the canister gases (Fig. 6A) suggested some possible differences between the flame zones. The previously published wind tunnel data where the sample taken directly in front of the spreading flame from a similar pine needle bed will be referred to as the “pre-flame” zone. The order of the relative values on some gases appeared to change. The measured amounts of many of the hydrocarbons, CO and H_2 increased appreciably from the pre-flame zone to the persistent flame zone while the relative amount of CO_2 decreased. This is consistent with the model in Fig. 1 (zone IIa, IIb, III and IV) due to the rate of pyrolysis increasing as the spreading flame approached heating the unburnt fuel. The relative amounts of all gases except CO_2 decreased from the persistent zone to the intermittent zone. The intermittent zone is not shown in Fig. 1; however, it has been described as the zone where “clumps of flame are seen to rise periodically from the continuous flame zone with a regular frequency of a few Hz” [50]. This intermittency would result in a lower quantity of flame gases being sampled relative to CO_2 which has a higher concentration in the atmosphere. The intermittency could be a result of an increasing stoichiometric air/fuel mass ratio and/or fluid dynamics related by turbulence, vorticity and entrainment [44,49,102,103]. The relative amount of many gases in the plume either decreased further or were similar to the intermittent zone.

For the FTIR data set (Table 3) which contained 9 fires, H_2O, CO_2 and CO had the greatest mixing ratios in all three flame zones. In addition to measuring some of the same hydrocarbons that were identified in the canister GC samples, the FTIR data set contained several oxygenated

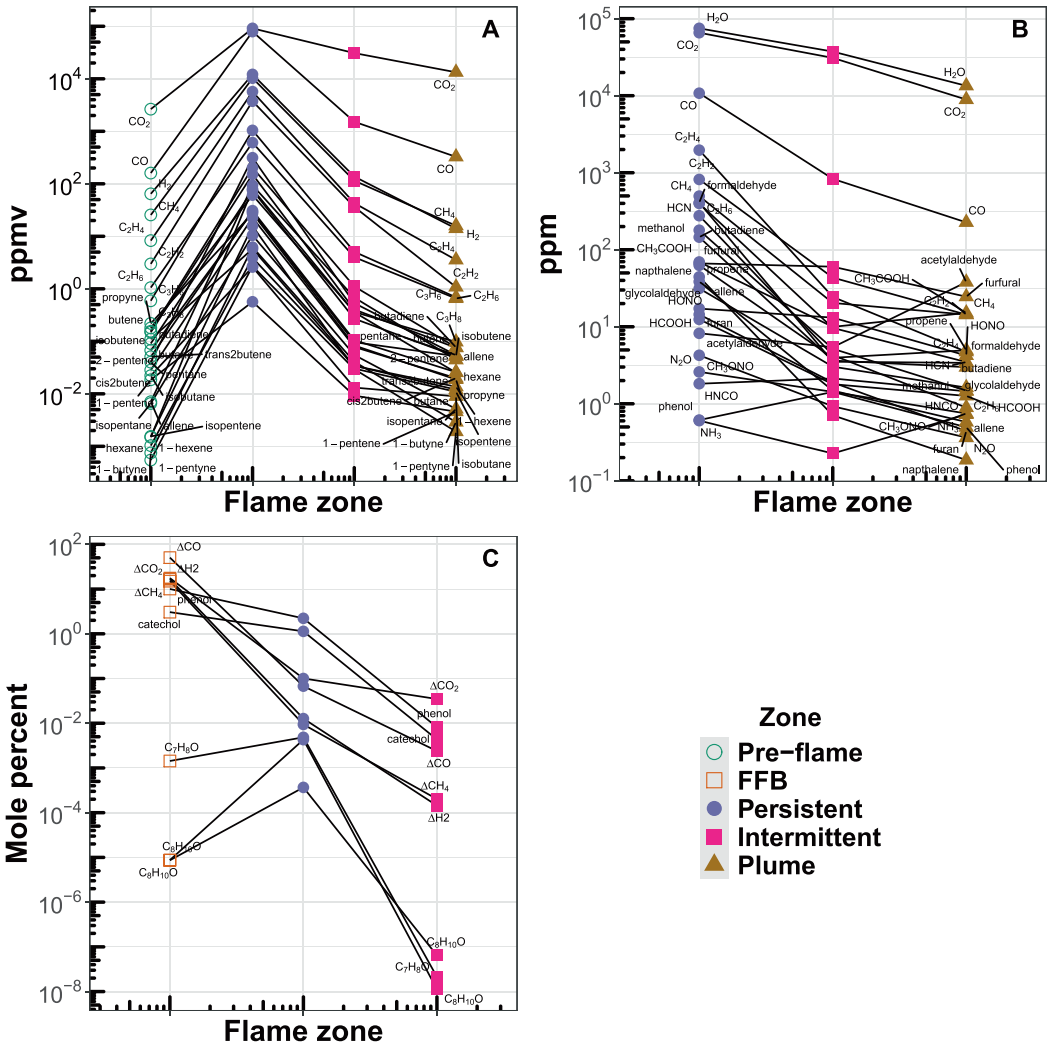

Fig. 6. Measured gases and tars in different zones of a diffusion flame in longleaf pine needles (A) from canister samples analyzed by GC/MS, (B) static samples measured by FTIR spectroscopy and (C) tar samples determined by GC/MS. Note that the pre-flame samples (A) were collected in advance of the flame in a wind tunnel [65] and the FFB samples (C) were generated by heating the needles in the post-flame hot gases of a flat flame burner [46].

hydrocarbons as well as nitrogen compounds. Mixing ratios in general decreased from persistent to intermittent to plume zone. The number of gases below detection limits also increased along this same gradient.

After imputation, the FTIR data set contained 9 observations of 26 gases. On a relative basis (Table 6), H_2O and CO_2 comprised 97 percent of the mean gas composition measured by FTIR while CO comprised 2 percent. Similarly, H_2O and CO_2 accounted for 94 percent of the total variance while CO accounted for 4.9 percent. The relative amount of H_2O and CO_2 did not appear to change between the flame zones while CO decreased from the persistent flame to the intermittent flame and plume zones (Fig. 6B). The relative amounts of several gases decreased between the persistent and intermittent zones while other gases increased.

Quantitative tar yields were not measured, although the largest amount of tar was collected at the flame base, followed by tar from the intermittent zone. Only a negligible amount of tar was collected in the plume, likely due to low concentration in the plume due to entrainment and/or combustion. Thirty-four tar compounds were identified in the persistent and intermittent zones (Table 4) in a total of 9 fires. The samples from the plume zone did not contain any detectable compounds. Eighty percent of the tars in the persistent zone were aromatic while only 29 percent were observed in the intermittent zone. In the absence of O_2 and as gas temperature increased, one would expect the tar to either (a) polymerize to form higher molecular weight compounds, eventually forming soot, or (b) crack to form lower molecular weight compounds. In the intermittent zone, however, it was likely that O_2 was in contact with the pyrolysis products, and oxidation of these pyrolysis products occurred. The lower aromatic content of the tars from this analysis suggested that either the aromatic tars were cracked or oxidized preferentially to non-aromatic species, or that the tars formed aromatic species that were of higher molecular weight than could be analyzed in the GC/MS system. Tar samples collected in the persistent zone were rich in phenolic compounds (Table 4). Following the general trend of decrease in concentration of aromatic compounds as sampling height increased, mole percent of phenolic compounds decreased as the sampling height increased. Twenty-one percent of aromatics present in the persistent zone contained phenolic compounds while almost no phenolic compounds were detected in the intermittent zone. Ethyl *iso*-allocholate was the only tar identified in all 9 fires. With the large 95 percent confidence intervals around the geometric means for the tars due in part to the small sample size, it is premature to draw conclusions about differences in tar composition between the flame zones even though trends are suggested by the mole percent plot (Fig. 6C). More tar compounds were observed in the persistent flame zone than in the intermittent zone (Table 4). Of the tars identified previously in the high heating rate FFB [46] data sets, only nine were measured in the present

Table 6
Compositional summary statistics for excess mixing ratio (ppm_v) of gases determined by FTIR spectroscopy. CO_2, CO, CH_4, H_2O are excess mixing ratios adjusted for atmospheric concentrations and humidity.

	Center	Variance contribution[a]
Water (H_2O)	5.39E-01	5.1E+01
Carbon dioxide (CO_2)	4.34E-01	4.3E+01
Carbon monoxide (CO)	2.10E-02	4.9E+00
Acetylene (C_2H_2)	1.30E-03	2.1E-02
Ethene (C_2H_4)	1.05E-03	1.7E-01
Methane (CH_4)	7.86E-04	2.8E-01
Furfural ($C_5H_4O_2$)	7.33E-04	3.7E-04
Hydrogen cyanide (HCN)	3.82E-04	1.1E-02
Acetic acid (CH_3COOH)	3.00E-04	2.3E-03
Formaldehyde (HCHO)	2.45E-04	8.3E-03
Methanol (CH_3OH)	1.84E-04	1.2E-03
Ethane (C_2H_6)	1.74E-04	3.1E-03
1,3-butadiene (C_4H_6)	1.71E-04	1.5E-03
Nitrous acid (HONO)	1.61E-04	2.4E-05
Propene (C_3H_6)	1.50E-04	9.0E-03
Acetaldehyde (CH_3CHO)	1.38E-04	3.7E-03
Glycolaldehyde ($C_2H_4O_2$)	8.27E-05	5.9E-04
Allene (C_3H_4)	5.12E-05	7.0E-05
Formic acid (HCOOH)	4.56E-05	4.7E-05
Furan (C_4H_4O)	3.88E-05	2.6E-04
Naphthalene ($C_{10}H_8$)	3.00E-05	1.1E-04
Isocyanic acid (HNCO)	2.67E-05	4.2E-06
Methyl nitrite (CH_3ONO)	2.17E-05	7.3E-07
Nitrous oxide (N_2O)	1.80E-05	3.0E-07
Phenol (C_6H_6O)	1.22E-05	6.1E-07
Ammonia (NH_3)	5.84E-06	4.2E-06

a.Percentage of variation that the gas contributed to the total variance (totvar), totvar = 0.025.

Table 7
Compositional summary statistics for the relative amount of tar compounds sampled from a diffusion flame in longleaf pine needles. The sampling method did not capture any tars in the plume zone. All compounds are solid at ambient conditions.

Tar compound[a]	Center	Variance contribution[b]
Ethyl *iso*-allocholate	1.74E-01	3.6
$C_{26}H_{54}$	9.27E-02	1.4
Fluorene	7.41E-02	5.9
Caprolactam	7.02E-02	3.4
3-methylphenol	6.90E-02	0.9
Phenanthrene	5.81E-02	4.9
$C_{20}H_{18}O_2$	4.61E-02	0.6
Biphenylene	4.51E-02	2.8
Phenol	4.04E-02	0.7
$C_{12}H_{15}N$	3.85E-02	4.3
$C_{11}H_{10}$	3.25E-02	7.8
$C_{20}H_{38}O_2$	2.89E-02	0.8
Acenaphthylene	2.86E-02	2.1
Catechol	2.77E-02	0.4
C_8H_8O	2.68E-02	2.9
$C_9H_{10}O$	2.66E-02	2.3
1,2-benzothiazole	2.41E-02	4.9
Biphenyl	2.25E-02	7.3
2-ethenylnaphthalene	1.58E-02	4.9
4-ethylphenol	1.40E-02	1.8
$C_{14}H_{24}O$	1.29E-02	1.8
$C_{37}H_{76}O$	9.87E-03	10.6
Propoxur	6.57E-03	0.9
2-methylphenol	4.96E-03	2.4
Secalciferol	2.31E-03	8.2
$C_{25}H_{32}O_8$	2.03E-03	0.4
1-methylideneindene	1.95E-03	1.2
3,4-dimethylphenol	1.77E-03	6.2
$C_{25}H_{42}O_2$	1.64E-03	2.2
$C_{20}H_{28}O_6$	5.32E-04	2.5

a.Refer to Table 4 for names and chemical formulae.
b.Percentage of variation that the gas contributed to the total variance (totvar), totvar = 30.7.

data set.

After imputing values to replace the BDL values, the tar data set had 16 observations and 19 compounds that occurred in more than 20 percent of the observations (Table 7). The relative amount of ethyl *iso*-allocholate in the mean composition (center) was largest followed by $C_{26}H_{54}$, fluorene, caprolactam and 3-methylphenol. $C_{37}H_{76}O$, secalciferol, $C_{11}H_{10}$ and biphenyl accounted for 34 percent of the total variance. The amounts of some tars increased while other tars decreased when all three flame zones were considered (Fig. 6C).

The average molecular weight of the compositions by zone was estimated for the tar data set by multiplying the center (mean) of the composition for each zone (not shown) by the molecular weights. The mean molecular weight of the tars reported in the FFB pyrolysis data set was 133.86 [46] while the mean molecular weight of identified tars in the present study was 200.53 and 287.88 for the persistent and intermittent flame zones, respectively. The increase in molecular weight from the persistent zone to the intermittent zone is consistent with the pathway to soot formation [104] which is important for flame radiation and fine particulate matter ($PM_{2.5}$) in smoke.

3.2. Principal components analysis (PCA) and PERMANOVA

For the canister data, a plot of the first two principal components suggested potential differences in the gas composition of the flame zones (Fig. 7A). The persistent flame zone composition appeared to be distinct from the other three zones. The intermittent and plume zones overlapped appreciably and many of the pre-flame observations fell outside of the 95 percent confidence ellipses about the persistent, intermittent and plume zone means. The PERMANOVA indicated that the flame zone was statistically significantly associated with the canister gas composition ($p = 0.001$). The six pairwise comparisons also indicated that the mean canister gas composition in the four flame zones (persistent, intermittent, plume and pre-flame) each significantly differed from the others (FDR-adjusted $p < 0.004$).

Due to the small sample size for the FTIR data set, a 95 percent confidence ellipse about the mean composition could only be estimated for the intermittent flame zone (Fig. 7B). Both measurements from the plume zone fell within this ellipse while the three measurements from the persistent flame zone fell outside of the confidence ellipse, suggesting that the observed persistent flame gas composition differed from the other two flame zones.

Like the FTIR data set, due to the small size of the tar data set, a 95 percent confidence ellipse could only be constructed for the persistent flame zone (Fig. 7C). All intermittent flame zone data points fell outside of this ellipse suggesting a difference in tar composition between the zones.

3.3. Flame zone effects

The canister data set consisted primarily of unoxygenated hydrocarbons (Table 2). The nine tailored balances for this data set compared the relative amount of CO and CO_2 to all hydrocarbons, the amount of CO to CO_2, the amount of saturated hydrocarbons (CH_4, C_2H_6, C_3H_8, C_4H_{10}, C_5H_{12}, C_6H_{14}) to unsaturated hydrocarbons, and the amount of each saturated hydrocarbon relative to its pyrolysis products. For example, the balance for CH_4 formed a log-ratio $\tilde{z}_{CH_4}$ that compared the relative amount of CH_4 to the relative amounts of H_2 and C_2H_6. Similarly, the balance $\tilde{z}_{C_2H_6}$ compared the amount of C_2H_6 with H_2, C_2H_4, C_2H_2 and C_4H_6 (Table 8). If a balance's value was greater than zero, the numerator was relatively larger than the denominator and vice-versa when the value was less than zero. The Kruskal-Wallis test suggested that the median values for eight of the nine balances statistically differed significantly between flame zones ($p < 0.003$) (Fig. 8). The p-value for the Kruskal-Wallis test of the balance of saturated hydrocarbons to unsaturated hydrocarbons was 0.054 which did not meet the *a priori*

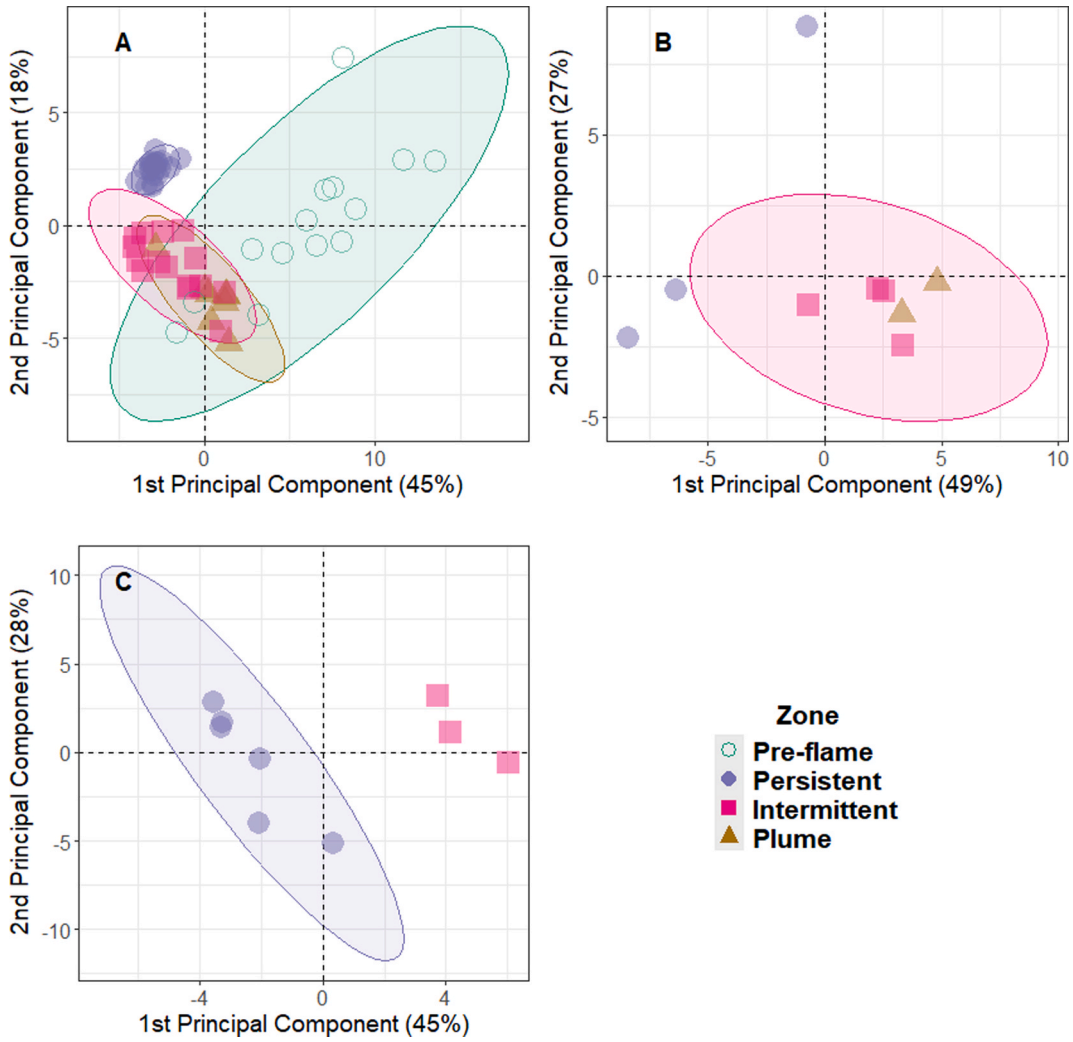

Fig. 7. Measurements of gas concentrations represented in the first two principal components (PCs) space suggesting differences in gas composition between zones of a diffusion flame from longleaf pine needles. Measured gases were from (A) canister samples analyzed by GC/MS, (B) static samples measured by FTIR spectroscopy and (C) tar samples determined by GC/MS. Note that the pre-flame samples were collected in advance of the flame in a wind tunnel [65]. The ellipses are 95 percent confidence ellipses about each zone mean.

significance criteria established. This balance estimated the relative reactivity of the mixture; saturated hydrocarbons are less reactive than unsaturated hydrocarbons, so reactivity increases as the balance decreases. In all cases, the balance value was greater than 1 indicating that relatively more saturated hydrocarbons were present in all zones suggesting that the gas mixture had lower volatility. For the other balances, at least one of the flame zone median values differed from the others (Table 7).

Examining the median values for the balance of CO_2 and CO with all hydrocarbons, there was relatively less CO and CO_2 in the persistent flame compared with the other zones and in the intermittent flame compared with the plume (difference in balance values < 0). For the same balance, the plume had more CO and CO_2 than the pre-flame zone. More CO relative to CO_2 was measured in the persistent zone compared to the other zones (difference in balance values > 0); the intermittent zone also had more CO relative to CO_2 in the plume. Significantly less ethane, propane, and butane relative to their pyrolysates and more pentane and hexane relative to their pyrolysates were measured in the persistent zone than in the plume. Less methane relative to H_2 and C_2H_6 and more pentane relative to its pyrolysates were found in the persistent zone compared to the intermittent zone. In most comparisons, more hexane and pentane relative to their pyrolysates were measured in the persistent flame zone compared to the other flame zones.

Many pyrolysis experiments have been performed at slow heating rates and low temperatures, such as in a thermogravimetric analyzer (TGA), to determine the product yields, composition and kinetics associated with wildland fuels. Some fast pyrolysis experiments [e.g., 17] have used heating rates observed in wildland fires and found differences in gas composition between non-oxidizing (fuel rich flat flame burner) and ambient atmosphere (wildland flame) environments; the difference between composition was mainly attributed to the CO-CO_2 log-ratio.

In the present study, the experiments measured an open burning wildland fuel flame with realistic flame temperatures and heating rates [65]. Some wildland fire simulation efforts have started to include combustion schemes with simple representative, often global, gas compositions [16,105,106]. Others are attempting to model smoke formation [107,108] rather than using an empirical smoke yield (emission factor) as in [109]. The heat of combustion changes with location due to the change in gas and tar species as well. Such improvements to simulations will require measurements of gas and tar yields and species within different areas of a flame.

The chemical composition of a wildland flame is complex and dynamic. From a simple mass balance using the ultimate analysis results and assuming complete combustion of the pine needles (based on observing only residual inorganic ash in the experimental fires), 1 kg of dry needles would yield 1.92 kg CO_2 and 0.54 kg H_2O. Assuming pine

Table 8
Summary of pairwise comparisons of selected log-ratio balances of gases collected in canisters by flame zone. ** indicates adjusted p-value ≤ 0.05.

Balance	Pairwise Comparison[a] Per-Int	Per-Plm	Per-Prf	Int-Plm	Int-Prf	Plm-Prf
CO, CO_2 vs all hydrocarbons	−3.8**	−4.6**	−3.1**	−0.8**	0.6	1.5**
CO vs CO_2	1.9**	2.3**	1.6**	0.4**	−0.3	−0.6
Saturated vs unsaturated	0.0	−0.6	−0.5	−0.6	−0.5	0.1
CH_4 vs pyrolysates[b] $\left(\widetilde{z}_{CH_4}\right)$	−0.2**	−0.2	0.3	0.0	0.5**	0.5
$\widetilde{z}_{C_2H_6}$	0.4	−0.6**	0.2	−0.9**	−0.2	0.7
$\widetilde{z}_{C_3H_8}$	0.4	−0.9**	−0.3**	−1.3**	−0.6**	0.7
$\widetilde{z}_{C_4H_{10}}$	0.2	−1.9**	−2.5**	−2.1**	−2.8**	−0.7**
$\widetilde{z}_{C_5H_{12}}$	1.4**	1.9**	3.0**	0.5	1.7**	1.2**
$\widetilde{z}_{C_6H_{14}}$	−0.1	1.2**	4.2**	1.3**	4.3**	3.0**

a.Per, Int, Plm, and Prf indicate persistent, intermittent, plume and pre-flame zones, respectively. Values are difference between flame zone median values for a balance $\left(\widetilde{z}_k\right)$. P-values adjusted to control false discovery rate [100].

b.Balance $\widetilde{z}_{C_xH_y}$ denotes the log-ratio balance between a saturated hydrocarbon C_xH_y (numerator) and its pyrolysates (denominator). Pyrolysates are those gases which could be produced by pyrolysis of the saturated hydrocarbon. The saturated hydrocarbons CH_4, C_2H_6, C_3H_8, C_4H_{10}, C_5H_{12} and C_6H_{14} had 2, 4, 9, 14, 21, and 24 of the measured unsaturated hydrocarbons, respectively, as pyrolysates.

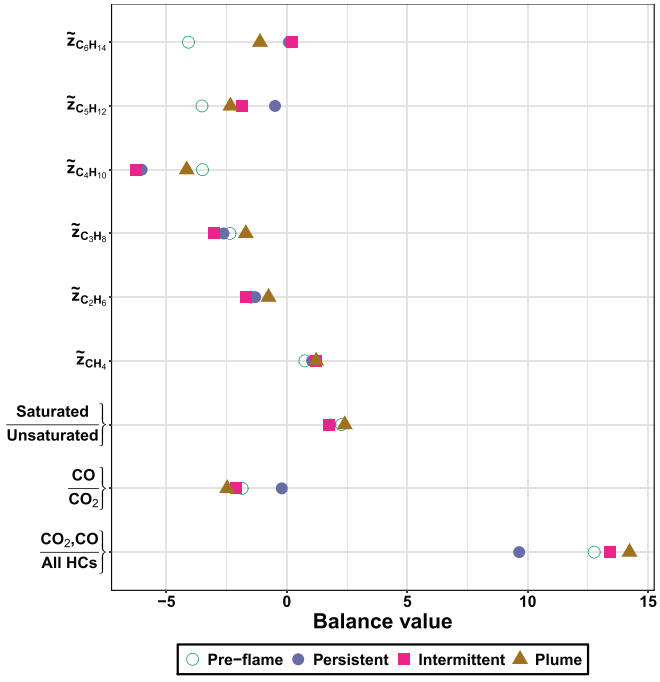

Fig. 8. Comparison of median values for selected log-ratio balances $\left(\widetilde{z}_k\right)$ of gases collected in canisters by flame zone. Balance $\widetilde{z}_{C_xH_y}$ denotes the log-ratio balance (Eq. 2.3) between a saturated hydrocarbon C_xH_y and its pyrolysates. Statistically significant differences between zones for all balances except the saturated vs unsaturated balance according to Kruskal-Wallis test (p-value < 0.003). Note that the pre-flame samples were collected in advance of the flame in a wind tunnel [65].

needle moisture content (dry weight basis) of 10 percent would yield 0.64 kg H_2O. The log-ratio based on CO_2 and H_2O ppm expressed as a balance, $\left[\frac{1}{\sqrt{2}}\ln(CO_2/H_2O)\right]$ [90], would be 0.896 and 0.777 for dry and 10 percent moisture content pine needles, respectively. For the excess mixing ratios for the FTIR (Table 3, Table 6) in the persistent flame zone, this log-ratio was −0.09 indicating that less CO_2 was produced in this zone relative to H_2O which indicates incomplete combustion which is further corroborated by the presence of the many C-bearing compounds, especially the CO. Note that the log-ratio in this instance is $\left[\frac{1}{\sqrt{2}}\ln(\Delta CO_2/\Delta H_2O)\right]$ where Δ indicates that the ambient ppm amounts were subtracted. The ambient mixing ratio for CO_2 was approximately 414 and ranged from 1612 to 3456 for H_2O based on the temperature and relative humidity which could affect the ratio. If values from the compositional center (Table 6) were used, $\left[\frac{1}{\sqrt{2}}\ln(\Delta CO_2/\Delta H_2O)\right] = -0.15$ indicating the same result. For the intermittent and plume zones (Table 3), $\left[\frac{1}{\sqrt{2}}\ln(\Delta CO_2/\Delta H_2O)\right]$ was −0.13 and −0.29, respectively. The mean log-ratios of the aggregated C gases to H_2O were −0.08, −0.11, and −0.26 for the persistent, intermittent and plume zones, respectively. This indicates that the amount of C decreased slightly in dominance relative to H_2O as distance from the combustion zone increased. However, the large variability in the FTIR measurements, particularly in H_2O and CO_2 (Table 3, Table 6) makes it difficult to determine how close the measurements were to the theoretical ratio. While it is standard practice to adjust measured smoke emissions for ambient conditions [110], appropriateness of this approach for measurements from a combustion zone is unknown. For instance, measurements of O_2 in a combustion zone should not be adjusted for obvious reasons.

Of the non-H_2O flame gases, CO_2 was the most dominant. Dominance can be quantified using different indices (Table 9). The ratio of CO_2 and CO has long been identified as an important index related to combustion efficiency or completeness [111]. Another commonly used index, modified combustion efficiency (MCE), defined as the ratio between CO_2 and the sum of CO and CO_2 [62,66,112] is constrained between 0 and 1. MCE has often been improperly correlated with smoke emissions in statistical analyses [87]. A CoDA-based index (the simple log-ratio between CO_2 and CO) can also describe the relative dominance of CO_2 to CO. These 3 measures changed between the different flame zones. In the persistent flame zone, more CO was present relative to CO_2 while more CO_2 relative to CO was observed in the other zones. In the FFB, less CO_2 relative to CO was observed compared to the persistent flame. It is important to note that the log-ratio of CO_2 and CO takes the relative nature of the compositional data into account. While it has been shown that the ratio of CO and CO_2 can be related to the amount of O_2 present, this has not been examined with the present data sets due to the challenge of comparing the O_2 time series with the time-integrated gas and tar samples.

Nitrous acid (HONO) is a gas of interest due to its impact on atmospheric chemistry. Several studies have examined HONO formation in smoke plumes and in urban areas [113–116] and found a significant amount of HONO and other organic acids in "fresh" smoke. The presence of H_2O (as relative humidity) has been shown to have an effect on HONO formation on soot [117] so both the H_2O present in the air as well as the relatively large amount of H_2O measured in the persistent and intermittent zones may be important to consider in modeling. While soot was not measured in this study, it is a well-known constituent of the flame and smoke [42]. In experiments conducted at the Forest Service's Missoula Fire Sciences Laboratory, "fresh" smoke was typically collected 15 m above a burning fire approximately 5 s after being emitted from the flame. While the FTIR sample size was relatively small in the present study, the FTIR measurements documented the presence of HONO at

Table 9
Measures of dominance of CO_2 in gas composition by flame zone for different data sources.

				Flame Zone		
Measure	Method[d]	Pre-flame[e]	FFB	Persistent	Intermittent	Plume
CO_2/CO [a]	Canister	16.49		1.16	20.32	40.80
	FTIR			6.09	37.21	39.35
	Tars[f]		0.35	1.49	14.60	
$CO_2/(CO + CO_2)$ [b]	Canister	0.94		0.54	0.95	0.98
	FTIR			0.86	0.97	0.98
	Tars		0.26	0.60	0.94	
$\frac{1}{\sqrt{2}}\ln(CO_2/CO)$ [c]	Canister	1.98		0.10	2.13	2.62
	FTIR			1.28	2.56	2.60
	Tars		−0.75	0.28	1.90	

a.Using mole ratio [112].
b.Using modified combustion efficiency [113].
c.Using simple log-ratio approach.
d.Canister and FTIR methods used excess mixing ratios (adjusted for ambient atmospheric concentrations while the FFB measurements were adjusted to account for the CO and CO_2 content of the post-flame gases in the flat-flame burner.
e.Pre-flame canister samples were collected in advance of the flame in a wind tunnel [65].
f.For the Tars data set CO and CO_2 values from [46] were used to estimate the FFB values and CO and CO_2 from the canister data for the subset of fires where tars were collected were used to estimate the persistent and intermittent flame zone values.

Table 10
Comparison of the molar fractions of common gases sampled in pyrolysis and various locations in and adjacent to a diffusion flame for two pine species.

Source	CO_2	CO	CH_4	C_2H_4	C_3H_6	C_2H_6	C_4H_6	C_4H_8	C_3H_8	C_4H_{10}	$\sum C_xH_y/CO$ [d]
Pinus pinaster[a]	0.64	0.21	0.04	0.008	0.001	0.014	0.054	0.018	0.009	0.005	0.69
Pinus palustris											
Persistent[b] − Canisters	0.48	0.42	0.05	0.030	0.006	0.003	0.001	0.001	3.E-04	4.E-05	0.23
Persistent − FTIR	0.82	0.11	0.03	0.02	0.004	0.003	0.001	0	0.02	0	0.73
Intermittent	0.95	0.05	0.00	0.001	2.E-04	1.E-04	5.E-05	3.E-05	1.E-05	2.E-06	0.11
Plume	0.97	0.02	0.00	3.E-04	5.E-05	5.E-05	1.E-05	2.E-05	7.E-06	3.E-06	0.07
Wind tunnel[c] − Canisters	0.73	0.06	0.01	0.004	2.E-04	4.E-04	7.E-05	8.E-05	7.E-05	1.E-04	0.20
Wind tunnel − FTIR	0.92	0.07	0.003	0.003	6.E-04	1.E-04	1.E-04	0	0	0	0.09

a.Data for crushed *Pinus pinaster* needles. [121].
b.Data from this paper.
c.Data for *Pinus palustris* needles from wind tunnel measurements in advance of flame. [65].
d.Ratio of sum of hydrocarbon mole fractions to CO mole fraction.

higher concentrations in the persistent and intermittent flame zones. The average temperatures in these two zones were more than 400 °C (673 K). There are not sufficient chemical species data to speculate on the exact reaction or reactions that formed HONO; the NIST Kinetics database [118] lists over 448 possible reactions that produce HONO. These results show HONO formation in the flame in addition to prior measurements of HONO in the smoke column [113,114,119].

Comparison of the results from the present experiment with experimental mixtures measured in a tube furnace [120] which were used to formulate a global kinetic model [16] showed similarities and differences. The gases were emitted by a Mediterranean pine (*Pinus pinaster* Aiton) and two shrub species (*Erica arborea* L., *Cistus monspeliensis* L.): CO, CO_2, H_2O, along with saturated and unsaturated hydrocarbons CH_4, C_2H_4, C_2H_6, C_3H_6, C_3H_8, C_4H_6, C_4H_8, and C_4H_{10}. Of these gases, a subcomposition of 10 was also measured in the present study (Table 2, Table 3) and in pre-flame samples in a wind tunnel [65,121]. For the pines (Table 10), visual inspection of the mole percents suggested that the amount of CO in Tihay et al.'s results [120] fell between the amount in the canister and FTIR samples of the persistent flame. Measurements of CO in other portions of the flame were similar. Pérez-Ramirez et al. [16], used the ratio of hydrocarbons to CO to formulate the experimental mixture to calibrate their global model. The ratio for the FTIR samples in the persistent zone (0.73) is similat to their data (0.69); however, the ratio for the canister data in the persistent zone is much smaller (0.23) due to the presence of a relatively greater mole fraction of CO. It is important to remember that the mole fractions reported in this table are relative and will change if other gases were added or removed [87]; this supports the need to use statistical methods that are appropriate to the nature of the data.

Assuming that the oxygen sensor values were accurate, the lack of oxygen in the persistent flame zone would indicate that this is a fuel rich, oxygen-deficient region corresponding to the "fuel rich interior" of Fig. 1. Oleoresins are resins, waxes, fats and fatty oils that are produced by plants and include alcohols, aldehydes, ketones, acids, and esters. Fragmentation of the oleoresins into C_2H_2 units is suggested in the model in zone III. The canister and FTIR samples showed decreases in the relative amount of C_2H_2 from the persistent flame zone to the plume zone with corresponding increases in CO_2 and H_2O which is consistent with the production and combustion of C_2H_2. We note that this is congruous with the time-resolved FTIR measurements of [78] in which C_2H_4 was rapidly generated and consumed during the pyrolysis and combustion phases, respectively. Several alcohols, aldehydes, ketones, acids, and esters were also observed in the gas and tar measurements supporting the conceptual model of the appearance of these partially oxidized organics; however, due to the small sample size for the tar and FTIR samples, it was not possible to determine differences between flame zones. More of the aromatic compounds were detected in the tar samples from the persistent zone as expected. The increased relative amounts and higher molecular weight compounds suggest synthesis of the aromatic compounds as indicated in zone V occurring in the persistent and intermittent flame zones. While the Ward model is qualitative in nature, many of its components are supported by the data in this paper. Further validation of this model is planned with new, more detailed gas and particulate data.

4. Conclusions

While the present study was fundamentally exploratory, the data

suggest meaningful differences in the gaseous composition between the three zones of the flame. The mole fractions of hydrocarbons relative to CO and CO_2 decreased from the persistent flame zone above the pyrolyzing needles through the intermittent flame zone into the flame-free plume. The concentration of tars also decreased over this same gradient which could result from chemical reactions occurring in the flame as well as air entrainment into the flame/plume. Partial agreement of the gas composition in the persistent flame zone with the gas composition used to formulate a global kinetic model of the combustion of evolved gases in a wildland fire provides support for the future use of this kinetics model in physically based fire models in U.S. wildland fuels. The identification of different gases and tars in the different flame zones supported the conceptual model of a wildland flame formulated by Ward. More detailed and synchronized measurements of gas and particulate composition in these flame zones are underway to improve physically based fire models.

CRediT authorship contribution statement

David.R. Weise: Writing – original draft, Project administration, Funding acquisition, Formal analysis, Conceptualization. **Thomas H. Fletcher:** Writing – review & editing, Formal analysis, Data curation. **Timothy J. Johnson:** Writing – review & editing, Formal analysis, Data curation. **WeiMin Hao:** Writing – review & editing, Formal analysis, Data curation. **Russell G. Tonkyn:** Writing – review & editing, Formal analysis, Data curation. **Catherine A. Banach:** Writing – review & editing, Formal analysis, Data curation. **Javier Palarea-Albaladejo:** Writing – review & editing, Formal analysis. **Mahsa Alizadeh:** Writing – review & editing, Formal analysis, Data curation. **Stephen Baker:** Writing – review & editing, Formal analysis, Data curation.

Declaration of competing interest

The authors declare that they have no known competing financial interests or personal relationships that could have appeared to influence the work reported in this paper.

Funding Acknowledgement

This work was supported by the DOD/DOE/EPA Strategic Environmental Research and Development Program project RC-2640. JPA was supported by the project PID2021-123833OB-I00, funded by the Spanish Ministry of Science and Innovation (MCIN/AEI/10.13039/501100011033) and by ERDF A way of making Europe. USDA Forest Service annual research appropriations provided in-kind support from 2016-2025.

Appendix A. Supplementary data

Supplementary data to this article can be found online at https://doi.org/10.1016/j.fuel.2025.136681.

Data availability

Weise, David R.; Fletcher, Thomas H.; Johnson, Timothy J.; Hao, WeiMin; Tonkyn, Russell G.; Banach, Catherine A.; Palarea-Albaladejo, Javier; Alizadeh, Mahsa; Baker, Stephen P. 2025. Gases measured in different diffusion flame zones. Fort Collins, CO: Forest Service Research Data Archive. https://doi.org/10.2737/RDS-2025-0055. Tar data embargoed in Alizadeh's dissertation.

References

[1] Drysdale D. An introduction to fire dynamics. 3rd ed. Chichester, West Sussex: Wiley; 2011.
[2] Bradbury AGW, Sakai Y, Shafizadeh F. A kinetic model for pyrolysis of cellulose. J Appl Polym Sci 1979;23:3271–80. https://doi.org/10.1002/app.1979.070231112.
[3] Leng E, Guo Y, Chen J, Liu S, Xue Y. A comprehensive review on lignin pyrolysis: Mechanism, modeling and the effects of inherent metals in biomass. Fuel 2022;309:122102. https://doi.org/10.1016/j.fuel.2021.122102.
[4] Sharma RK, Wooten JB, Baliga VL, Lin X, Geoffrey Chan W, Hajaligol MR. Characterization of chars from pyrolysis of lignin. Fuel 2004;83:1469–82. https://doi.org/10.1016/j.fuel.2003.11.015.
[5] Puri L, Hu Y, Naterer G. Critical review of the role of ash content and composition in biomass pyrolysis. Front Fuels 2024;2:1378361. https://doi.org/10.3389/ffuel.2024.1378361.
[6] Ward DE. Combustion chemistry and smoke. In: Johnson EA, Miyanishi K, editors. Forest Fires: Behavior and Ecological Effects. San Diego, CA: Academic Press; 2001. p. 55–77. https://doi.org/10.1016/B978-012386660-8/50006-3.
[7] Sparks TL, Wagner J. Composition of particulate matter during a wildfire smoke episode in an urban area. Aerosol Sci Tech 2021;55:734–47. https://doi.org/10.1080/02786826.2021.1895429.
[8] Hosseini S, Urbanski SP, Dixit P, Qi L, Burling IR, Yokelson RJ, et al. Laboratory characterization of PM emissions from combustion of wildland biomass fuels: particle emissions from biomass burning. J Geophys Res Atmospheres 2013;118:9914–29. https://doi.org/10.1002/jgrd.50481.
[9] Pyne SJ. World fire: the culture of fire on earth. Pbk. ed. Seattle: University of Washington Press; 1997.
[10] Prasad S, Yadav KK, Kumar S, Pandita P, Bhutto JK, Alreshidi MA, et al. Review on biofuel production: Sustainable development scenario, environment, and climate change perspectives – a sustainable approach. J Environ Chem Eng 2024;12:111996. https://doi.org/10.1016/j.jece.2024.111996.
[11] Demirbaş A. Biomass resource facilities and biomass conversion processing for fuels and chemicals. Energy Convers Manag 2001;42:1357–78. https://doi.org/10.1016/S0196-8904(00)00137-0.
[12] Demirbaş A. Combustion characteristics of different biomass fuels. Prog Energy Combust Sci 2004;30:219–30. https://doi.org/10.1016/j.pecs.2003.10.004.
[13] Demirbaş A. Mechanisms of liquefaction and pyrolysis reactions of biomass. Energy Convers Manag 2000;41:633–46. https://doi.org/10.1016/S0196-8904(99)00130-2.
[14] Liu C, Yan B, Chen G, Bai XS. Structures and burning velocity of biomass derived gas flames. Int J Hydrog Energy 2010;35:542–55. https://doi.org/10.1016/j.ijhydene.2009.11.020.
[15] Varghese RJ, Kolekar H, Kumar S. Laminar burning velocities of H2/CO/CH4/CO2/N2 -air mixtures at elevated temperatures. Int J Hydrog Energy 2019;44:12188–99. https://doi.org/10.1016/j.ijhydene.2019.03.103.
[16] Pérez-Ramirez Y, Santoni P, Darabiha N, Leroy-Cancellieri V, Leoni E. A global kinetic model for the combustion of the evolved gases in wildland fires. Combust Sci Technol 2012;184:1380–94. https://doi.org/10.1080/00102202.2012.691585.
[17] Weise DR, Fletcher TH, Johnson TJ, Hao WM, Dietenberger M, Princevac M, et al. Comparing gas composition from fast pyrolysis of live foliage measured in bench-scale and fire-scale experiments. Int J Wildland Fire 2024;33:WF23200. https://doi.org/10.1071/WF23200.
[18] Smith DA, Cox G. Major chemical species in buoyant turbulent diffusion flames. Combust Flame 1992;91:226–38. https://doi.org/10.1016/0010-2180(92)90055-T.
[19] Orloff L, De Ris J, Delichatsios MA. Chemical effects on molecular species concentrations in turbulent fires. Combust Flame 1987;69:273–89. https://doi.org/10.1016/0010-2180(87)90121-0.
[20] Adetona O, Reinhardt TE, Domitrovich J, Broyles G, Adetona AM, Kleinman MT, et al. Review of the health effects of wildland fire smoke on wildland firefighters and the public. Inhal Toxicol 2016;28:95–139. https://doi.org/10.3109/08958378.2016.1145771.
[21] Chen H, Samet JM, Bromberg PA, Tong H. Cardiovascular health impacts of wildfire smoke exposure. Part Fibre Toxicol 2021;18:2. https://doi.org/10.1186/s12989-020-00394-8.
[22] Crutzen PJ, Heidt LE, Krasnec JP, Pollock WH, Seiler W. Biomass burning as a source of atmospheric gases CO,H_2, $N_2$0, NO, CH_3Cl and COS. Nature 1979;282:253–6. https://doi.org/10.1038/282253a0.
[23] Curry JR, Fons WL. Forest-fire behavior studies. Mech Eng 1940;62:219–25.
[24] Raven PH, Evert RF, Curtis H. Biology of plants. 3rd ed. New York, N.Y: Worth Publishers; 1981.
[25] Zhang L, Larsson A, Moldin A, Edlund U. Comparison of lignin distribution, structure, and morphology in wheat straw and wood. Ind Crop Prod 2022;187:115432. https://doi.org/10.1016/j.indcrop.2022.115432.
[26] Matt FJ, Dietenberger MA, Weise DR. Summative and ultimate analysis of live leaves from southern U.S. forest plants for use in fire modeling. Energy Fuels 2020;20:4703. https://doi.org/10.1021/acs.energyfuels.9b04107.
[27] Collard F-X, Blin J. A review on pyrolysis of biomass constituents: mechanisms and composition of the products obtained from the conversion of cellulose, hemicelluloses and lignin. Renew Sustain Energy Rev 2014;38:594–608. https://doi.org/10.1016/j.rser.2014.06.013.
[28] Shafizadeh F. Introduction to the pyrolysis of biomass. J Anal Appl Pyrol 1982;3:283–305. https://doi.org/10.1016/0165-2370(82)80017-X.
[29] Jegers HE, Klein MT. Primary and secondary lignin pyrolysis reaction pathways. Ind Eng Chem Process Des Dev 1985;24:173–83. https://doi.org/10.1021/i200028a030.

[30] Caballero JA, Front R, Marcilla A, Conesa JA. Characterization of sewage sludges by primary and secondary pyrolysis. J Anal Appl Pyrol 1997;40–41:433–50. https://doi.org/10.1016/S0165-2370(97)00045-4.

[31] Patwardhan PR, Dalluge DL, Shanks BH, Brown RC. Distinguishing primary and secondary reactions of cellulose pyrolysis. Bioresour Technol 2011;102:5265–9. https://doi.org/10.1016/j.biortech.2011.02.018.

[32] Xiong Z, Han H, Azis MM, Hu X, Wang Y, Su S, et al. Formation of the heavy tar during bio-oil pyrolysis: a study based on Fourier transform ion cyclotron resonance mass spectrometry. Fuel 2019;239:108–16. https://doi.org/10.1016/j.fuel.2018.10.151.

[33] Zhou S, Garcia-Perez M, Pecha B, Kersten SRA, McDonald AG, Westerhof RJM. Effect of the fast pyrolysis temperature on the primary and secondary products of lignin. Energy Fuels 2013;27:5867–77. https://doi.org/10.1021/ef4001677.

[34] He Q, Guo Q, Umeki K, Ding L, Wang F, Yu G. Soot formation during biomass gasification: A critical review. Renew Sustain Energy Rev 2021;139:110710. https://doi.org/10.1016/j.rser.2021.110710.

[35] Alvarado MJ, Barsanti KC, Chung SH, Jaffe DA, Moore CT. Smoke Chemistry. In: Peterson DL, McCaffrey SM, Patel-Weynand T, editors. Wildland Fire Smoke in the United States. Cham, Switzerland: Springer International Publishing; 2022. p. 167–98. https://doi.org/10.1007/978-3-030-87045-4_6.

[36] Darley EF, Burleson FR, Mateer EH, Middleton JT, Osterli VP. Contribution of burning of agricultural wastes to photochemical air pollution. J Air Pollut Control Assoc 1966;16:685–90. https://doi.org/10.1080/00022470.1966.10468533.

[37] Prichard SJ, O'Neill SM, Eagle P, Andreu AG, Drye B, Dubowy J, et al. Wildland fire emission factors in North America: synthesis of existing data, measurement needs and management applications. Int J Wildland Fire 2020;29:132. https://doi.org/10.1071/WF19066.

[38] Clean Air Act. U.S. Code Title 42,Chapter 85, § 7491 et seq. 1970.

[39] Ottmar RD, Miranda AI, Sandberg DV. Characterizing Sources of Emissions from Wildland Fires. In: Bytnerowicz A, Arbaugh MJ, Riebau AR, Andersen C, editors. Wildland Fires and Air Pollution. Dev. Environ. Sci., 8. Elsevier; 2008. p. 61–78. https://doi.org/10.1016/S1474-8177(08)00003-X.

[40] Egolfopoulos FN, Hansen N, Ju Y, Kohse-Höinghaus K, Law CK, Qi F. Advances and challenges in laminar flame experiments and implications for combustion chemistry. Prog Energy Combust Sci 2014;43:36–67. https://doi.org/10.1016/j.pecs.2014.04.004.

[41] Westbrook CK, Dryer FL. Prediction of laminar flame properties of methanol-air mixtures. Combust Flame 1980;37:171–92. https://doi.org/10.1016/0010-2180(80)90084-X.

[42] Lobert JM, Warnatz J. Emissions from the combustion process in vegetation. In: Crutzen PJ, Goldammer JG, editors. Fire in the Environment: The Ecological, Atmospheric, and Climatic Importance of Vegetation Fires. Dahlem Workshop Report 13. John Wiley & Sons Ltd; 1993. p. 15–37.

[43] Ward DE. Particulate matter and aromatic hydrocarbon emissions from the controlled combustion of alpha pinene. University of Washington; 1979. Ph.D. thesis.

[44] Albini FA. A model for the wind-blown flame from a line fire. Combust Flame 1981;43:155–74. https://doi.org/10.1016/0010-2180(81)90014-6.

[45] Zukoski EE, Cetegen BM, Kubota T. Visible structure of buoyant diffusion flames. Symp Int Combust 1985;20:361–6. https://doi.org/10.1016/S0082-0784(85)80522-1.

[46] Safdari M-S, Rahmati M, Amini E, Howarth JE, Berryhill JP, Dietenberger M, et al. Characterization of pyrolysis products from fast pyrolysis of live and dead vegetation native to the southern United States. Fuel 2018;229:151–66. https://doi.org/10.1016/j.fuel.2018.04.166.

[47] Sekimoto K, Koss AR, Gilman JB, Selimovic V, Coggon MM, Zarzana KJ, et al. High- and low-temperature pyrolysis profiles describe volatile organic compound emissions from western US wildfire fuels. Atmospheric Chem Phys 2018;18:9263–81. https://doi.org/10.5194/acp-18-9263-2018.

[48] Shafizadeh F. The chemistry of pyrolysis and combustion. In: Rowell R, editor. Chem. Solid Wood, vol. 207, Washington, D.C.: American Chemical Society; 1984, p. 489–529. https://doi.org/10.1021/ba-1984-0207.ch013.

[49] Nelson Jr RM, Butler BW, Weise DR. Entrainment regimes and flame characteristics of wildland fires. Int J Wildland Fire 2012;21:127–40. https://doi.org/10.1071/WF10034.

[50] McCaffrey BJ. Purely buoyant diffusion flames: some experimental results. NBSIR 79-1910. Gaithersburg, MD: National Bureau of Standards; 1979.

[51] Bartoli P, Simeoni A, Biteau H, Torero JL, Santoni PA. Determination of the main parameters influencing forest fuel combustion dynamics. Fire Saf J 2011;46:27–33. https://doi.org/10.1016/j.firesaf.2010.05.002.

[52] Thomas JC, Hadden RM, Simeoni A. Experimental investigation of the impact of oxygen flux on the burning dynamics of forest fuel beds. Fire Saf J 2017;91:855–63. https://doi.org/10.1016/j.firesaf.2017.03.086.

[53] Bouhafid A, Vantelon JP, Joulain P, Fernandez-Pello AC. On the flame structure at the base of a pool fire. Symp Int Combust 1989;22:1291–8. https://doi.org/10.1016/S0082-0784(89)80140-7.

[54] Korobeinichev OP, Paletsky AA, Gonchikzhapov MB, Shundrina IK, Chen H, Liu N. Combustion chemistry and decomposition kinetics of forest fuels. Procedia Eng 2013;62:182–93. https://doi.org/10.1016/j.proeng.2013.08.054.

[55] Butler BW, Cohen J, Latham DJ, Schuette RD, Sopko P, Shannon KS, et al. Measurements of radiant emissive power and temperatures in crown fires. Can J For Res 2004;34:1577–87. https://doi.org/10.1139/x04-060.

[56] Amini E, Safdari M-S, DeYoung JT, Weise DR, Fletcher TH. Characterization of pyrolysis products from slow pyrolysis of live and dead vegetation native to the southern United States. Fuel 2019;235:1475–91. https://doi.org/10.1016/j.fuel.2018.08.112.

[57] Safdari M-S, Amini E, Weise DR, Fletcher TH. Heating rate and temperature effects on pyrolysis products from live wildland fuels. Fuel 2019;242:295–304. https://doi.org/10.1016/j.fuel.2019.01.040.

[58] Weise DR, Fletcher TH, Safdari M-S, Amini E, Palarea-Albaladejo J. Application of compositional data analysis to determine the effects of heating mode, moisture status and plant species on pyrolysates. Int J Wildland Fire 2022;31:24–45. https://doi.org/10.1071/WF20126.

[59] Alizadeh M, Weise DR, Fletcher TH. Characteristics of pyrolysis products of California chaparral and their potential effect on wildland fires. Fire 2024;7:271. https://doi.org/10.3390/fire7080271.

[60] Boardman CR, Dietenberger MA, Weise DR. Specific heat capacity of wildland foliar fuels to 434 °C. Fuel 2021;292:120396. https://doi.org/10.1016/j.fuel.2021.120396.

[61] Anderson HE, Rothermel RC. Influence of moisture and wind upon the characteristics of free-burning fires. Symp Int Combust 1965;10:1009–19. https://doi.org/10.1016/S0082-0784(65)80243-0.

[62] Yokelson RJ, Griffith DWT, Ward DE. Open-path Fourier transform infrared studies of large-scale laboratory biomass fires. J Geophys Res-Atmospheres 1996;101:21067. https://doi.org/10.1029/96JD01800.

[63] McMahon CK, Tsoukalas SN. Polynuclear aromatic hydrocarbons in forest fire smoke. Carcinogenesis 1978;3:61–73.

[64] Yokelson RJ, Burling IR, Gilman JB, Warneke C, Stockwell CE, de Gouw J, et al. Coupling field and laboratory measurements to estimate the emission factors of identified and unidentified trace gases for prescribed fires. Atmospheric Chem Phys 2013;13:89–116. https://doi.org/10.5194/acp-13-89-2013.

[65] Weise DR, Hao WM, Baker S, Princevac M, Aminfar A-H, Palarea-Albaladejo J, et al. Comparison of fire-produced gases from wind tunnel and small field experimental burns. Int J Wildland Fire 2022;31:409–34. https://doi.org/10.1071/WF21141.

[66] Ward DE, Radke LF. Emissions measurement from vegetation fires: a comparative evaluation of methods and results. In: Crutzen PJ, Goldammer JG, editors. Fire Environ. Ecol. Atmospheric Clim. Importance Veg. Fires Rep. Dahl. Workshop Held Berl. 15-20 March 1992, John Wiley & Sons Ltd.; 1993, p. 53–76.

[67] Schuette RD. Preparing reproducible pine needle fuel beds. Res. Note INT-36, Ogden, UT: USDA Forest Service, Intermountain Forest and Range Experiment Station; 1965.

[68] Fons WL, Bruce HD, Pong WY. A steady-state technique for studying the properties of free-burning wood fires. The Use of Models in Fire Research, Publication 786, Washington, D.C.: National Academy of Sciences. National Research Council 1961:219–34.

[69] Jenkins BM, Kennedy IM, Turn SQ, Williams RB, Hall SG, Teague SV, et al. Wind tunnel modeling of atmospheric emissions from agricultural burning: influence of operating configuration on flame structure and particle emission factor for a spreading-type fire. Environ Sci Technol 1993;27:1763–75. https://doi.org/10.1021/es00046a002.

[70] Moffat RJ. Gas Temperature Measurement. In: Dahl AI, editor. Temperature: Its Measurement and Control in Science and Industry, vol. 3 Part 2 Applied Methods and Instruments, New York: Reinhold Publishing Corporation; 1962, p. 553–71.

[71] Wotton BM, Gould JS, McCaw WL, Cheney NP, Taylor SW. Flame temperature and residence time of fires in dry eucalypt forest. Int J Wildland Fire 2012;21:270. https://doi.org/10.1071/WF10127.

[72] Blevins LG, Pitts WM. Modeling of bare and aspirated thermocouples in compartment fires. Fire Saf J 1999;33:239–59. https://doi.org/10.1016/S0379-7112(99)00034-X.

[73] EPA.. Compendium Method TO-14A Determination of volatile organic compounds (VOCs). In: ambient air using specially prepared canisters with subsequent analysis by gas chromatography. In: EPA/625/R-96/010b Compendium of Methods for the Determination of Toxic Organic Compounds in Ambient Air. 2nd ed. Cincinnati, OH: Environmental Protection Agency; 1999. p. 86.

[74] Colket MB, Naegeli DW, Dryer FL, Glassman I. Flame ionization detection of carbon oxides and hydrocarbon oxygenates. Environ Sci Technol 1974;8:43–6. https://doi.org/10.1021/es60086a007.

[75] Scharko NK, Oeck AM, Myers TL, Tonkyn RG, Banach CA, Baker SP, et al. Gas-phase pyrolysis products emitted by prescribed fires in pine forests with a shrub understory in the southeastern United States. Atmospheric Chem Phys 2019;19:9681–98. https://doi.org/10.5194/acp-19-9681-2019.

[76] Scharko NK, Oeck AM, Tonkyn RG, Baker SP, Lincoln EN, Chong J, et al. Identification of gas-phase pyrolysis products in a prescribed fire: first detections using infrared spectroscopy for naphthalene, methyl nitrite, allene, acrolein and acetaldehyde. Atmospheric Meas Tech 2019;12:763–76. https://doi.org/10.5194/amt-12-763-2019.

[77] Lindenmaier R, Scharko NK, Tonkyn RG, Nguyen KT, Williams SD, Johnson TJ. Improved assignments of the vibrational fundamental modes of *ortho-*, *meta-*, and *para*-xylene using gas- and liquid-phase infrared and Raman spectra combined with *ab initio* calculations: quantitative gas-phase infrared spectra for detection. J Mol Struct 2017;1149:332–51. https://doi.org/10.1016/j.molstruc.2017.07.053.

[78] Banach CA, Bradley AM, Tonkyn RG, Williams ON, Chong J, Weise DR, et al. Dynamic infrared gas analysis from longleaf pine fuel beds burned in a wind tunnel: observation of phenol in pyrolysis and combustion phases. Atmospheric Meas Tech 2021;14:2359–76. https://doi.org/10.5194/amt-14-2359-2021.

[79] Griffith DWT. MALT5 User guide. Version 5.5.9. 2016.

[80] Johnson TJ, Profeta LTM, Sams RL, Griffith DWT, Yokelson RL. An infrared spectral database for detection of gases emitted by biomass burning. Vib Spectrosc 2010;53:97–102. https://doi.org/10.1016/j.vibspec.2010.02.010.

[81] Sharpe SW, Johnson TJ, Sams RL, Chu PM, Rhoderick GC, Johnson PA. Gas-phase databases for quantitative infrared spectroscopy. Appl Spectrosc 2004;58:1452–61.
[82] Gordon IE, Rothman LS, Hill C, Kochanov RV, Tan Y, Bernath PF, et al. The HITRAN2016 molecular spectroscopic database. J Quant Spectrosc Radiat Transf 2017;203:3–69. https://doi.org/10.1016/j.jqsrt.2017.06.038.
[83] Archer MD. Genesis of the Nernst equation. In: Stock JT, Orna MV, editors. Electrochem. Past Present, vol. 390, Washington, DC: American Chemical Society; 1989, p. 115–26. https://doi.org/10.1021/bk-1989-0390.
[84] ECONOX SA. Operating manual: CarboProbe^{TM} 2021, 30 p.
[85] Stein SE. NIST/EPA/NIH Mass Spectral Library-PC Version. NIST Standard Reference Database 1A 1977. https://doi.org/10.18434/T4H594.
[86] Safdari MS. Characterization of Pyrolysis Products from Fast Pyrolysis of Live and Dead Vegetation. Dissertation. Brigham Young University, 2018.
[87] Weise DR, Palarea-Albaladejo J, Johnson TJ, Jung H. Analyzing wildland fire smoke emissions data using compositional data techniques. J Geophys Res Atmospheres 2020;125:e2019JD032128. https://doi.org/10.1029/2019JD032128.
[88] van den Boogaart KG, Delgado RT, Konsulke S. Chemical equilibria in compositional data. In: Pardo-Igúzquiza E, Guardiola-Albert C, Heredia J, Moreno-Merino L, Durán JJ, Vargas-Guzmán JA, editors. Mathematics of Planet Earth. Berlin, Heidelberg: Springer Berlin Heidelberg; 2014. p. 107–10. https://doi.org/10.1007/978-3-642-32408-6_26.
[89] Aitchison J. The statistical analysis of compositional data. London; New York: Chapman and Hall; 1986.
[90] Pawlowsky-Glahn V, Egozcue JJ, Tolosana-Delgado R. Modelling and analysis of compositional data. Chichester, West Sussex, U.K.: Wiley; 2015.
[91] R Core Team. R: A. Language and environment for statistical computing. Vienna, Austria: R Foundation for Statistical Computing; 2024.
[92] Larkin P. Chapter 2 - Basic Principles. In: Larkin P, editor. Infrared Raman Spectroscopy. Oxford: Elsevier; 2011. p. 7–25. https://doi.org/10.1016/B978-0-12-386984-5.10002-3.
[93] Little RJA, Rubin DB. Statistical analysis with missing data. Third edition. Hoboken, NJ: Wiley; 2020.
[94] Palarea-Albaladejo J, Antoni Martín-Fernández J, Ruiz-Gazen A, Thomas-Agnan C. lrSVD: an efficient imputation algorithm for incomplete high-throughput compositional data. J Chemom 2022;36:e3459. https://doi.org/10.1002/cem.3459.
[95] Dodder N. _OrgMassSpecR: Organic Mass Spectrometry_; R package version 0.5-3; 2017. https://doi.org/10.32614/CRAN.package.OrgMassSpecR.
[96] Mardia KV, Kent JT, Bibby JM. Multivariate analysis. London; New York: Academic Press; 1979.
[97] Anderson MJ. Permutational Multivariate Analysis of Variance (PERMANOVA). In: Balakrishnan N, Colton T, Everitt B, Piegorsch W, Ruggeri F, Teugels JL, editors. Wiley StatsRef Stat. Ref. Online, Chichester, UK: John Wiley & Sons, Ltd; 2017, p. 1–15. https://doi.org/10.1002/9781118445112.stat07841.
[98] Aitchison J, Greenacre M. Biplots of compositional data. J R Stat Soc Ser C Appl Stat 2002;51:375–92. https://doi.org/10.1111/1467-9876.00275.
[99] Herve M. RVAideMemoire: Testing and Plotting Procedures for Biostatistics 2023.
[100] Benjamini Y, Hochberg Y. Controlling the false discovery rate: a practical and powerful approach to multiple testing. J R Stat Soc B Methodol 1995;57:289–300. https://www.jstor.org/stable/2346101.
[101] Kirkwood TBL. Geometric means and measures of dispersion. Biometrics 1979;35:908–9. https://www.jstor.org/stable/2530139.
[102] Finney MA, Cohen JD, Forthofer JM, McAllister SS, Gollner MJ, Gorham DJ, et al. Role of buoyant flame dynamics in wildfire spread. Proc Natl Acad Sci 2015. https://doi.org/10.1073/pnas.1504498112. 201504498.
[103] Steward FR. Linear flame heights for various fuels. Combust Flame 1964;8:171–8. https://doi.org/10.1016/0010-2180(64)90063-X.
[104] Michelsen HA, Colket MB, Bengtsson P-E, D'Anna A, Desgroux P, Haynes BS, et al. A review of terminology used to describe soot formation and evolution under combustion and pyrolytic conditions. ACS Nano 2020;14:12470–90. https://doi.org/10.1021/acsnano.0c06226.
[105] Borujerdi PR, Shotorban B, Mahalingam S, Weise DR. Influence of pyrolysis gas composition and reaction kinetics on leaf-scale fires. Combust Sci Technol 2024;196:2356–79. https://doi.org/10.1080/00102202.2022.2135995.
[106] Mell W, Maranghides A, McDermott R, Manzello SL. Numerical simulation and experiments of burning douglas fir trees. Combust Flame 2009;156:2023–41. https://doi.org/10.1016/j.combustflame.2009.06.015.
[107] Liu Y, Kochanski A, Baker KR, Mell W, Linn R, Paugam R, et al. Fire behaviour and smoke modelling: model improvement and measurement needs for next-generation smoke research and forecasting systems. Int J Wildland Fire 2019;28:570–88.
[108] Lautenberger CW, de Ris JL, Dembsey NA, Barnett JR, Baum HR. A simplified model for soot formation and oxidation in CFD simulation of non-premixed hydrocarbon flames. Fire Saf J 2005;40:141–76. https://doi.org/10.1016/j.firesaf.2004.10.002.
[109] Lutes DE. FOFEM 6.7 first order fire effects model user guide. USDA Forest Service 2020.
[110] Yokelson RJ, Andreae MO, Akagi SK. Pitfalls with the use of enhancement ratios or normalized excess mixing ratios measured in plumes to characterize pollution sources and aging. Atmospheric Meas Tech 2013;6:2155–8. https://doi.org/10.5194/amt-6-2155-2013.
[111] Tsuchiya Y. CO/CO_2 ratios in fire. Fire Saf Sci 1994;4:515–26. https://doi.org/10.3801/IAFSS.FSS.4-515.
[112] Ward DE, Hao WM. Projections of emissions from burning of biomass for use in studies of global climate and atmospheric chemistry. Vancouver, British Columbia, Canada: Air and Waste Management Association; 1991. p. 19. https://www.fs.usda.gov/rm/pubs_journals/1991/rmrs_1991_ward_d001.pdf.
[113] Veres P, Roberts JM, Burling IR, Warneke C, de Gouw J, Yokelson RJ. Measurements of gas-phase inorganic and organic acids from biomass fires by negative-ion proton-transfer chemical-ionization mass spectrometry. J Geophys Res 2010;115:D23302. https://doi.org/10.1029/2010JD014033.
[114] Roberts JM, Veres P, Warneke C, Neuman JA, Washenfelder RA, Brown SS, et al. Measurement of HONO, HNCO, and other inorganic acids by negative-ion proton-transfer chemical-ionization mass spectrometry (NI-PT-CIMS): application to biomass burning emissions. Atmospheric Meas Tech 2010;3:981–90. https://doi.org/10.5194/amt-3-981-2010.
[115] Stadler D, Rossi MJ. The reactivity of NO2 and HONO on flame soot at ambient temperature: the influence of combustion conditions. PCCP 2000;2:5420–9. https://doi.org/10.1039/b005680o.
[116] Keene WC, Lobert JM, Crutzen PJ, Maben JR, Scharffe DH, Landmann T, et al. Emissions of major gaseous and particulate species during experimental burns of southern african biomass. J Geophys Res Atmospheres 2006;111:2005JD006319. https://doi.org/10.1029/2005JD006319.
[117] Kalberer M, Ammann M, Arens F, Gäggeler HW, Baltensperger U. Heterogeneous formation of nitrous acid (HONO) on soot aerosol particles. J Geophys Res Atmospheres 1999;104:13825–32. https://doi.org/10.1029/1999JD900141.
[118] Manion JA, Huie RE, Levin RD, Burgess DR Jr, Orkin VL, Tsang W, et al. NIST Chemical Kinetics Database, NIST Standard Reference Database 17, Version 7.0 (Web Version), Release 1.6.8, Data version 2015.09, Gaithersburg, Maryland: National Institute of Standards and Technology; 2015. https://kinetics.nist.gov/NIST .
[119] Burling IR, Yokelson RJ, Griffith DWT, Johnson TJ, Veres P, Roberts JM, et al. Laboratory measurements of trace gas emissions from biomass burning of fuel types from the southeastern and southwestern United States. Atmospheric Chem Phys 2010;10:11115–30. https://doi.org/10.5194/acp-10-11115-2010.
[120] Tihay V, Simeoni A, Santoni P-A, Rossi L, Garo J-P, Vantelon J-P. Experimental study of laminar flames obtained by the homogenization of three forest fuels. Int J Therm Sci 2009;48:488–501.
[121] Weise DR, Johnson TJ, Myers TL, Hao WM, Baker S, Palarea-Albaladejo J, et al. Comparing two methods to measure oxidative pyrolysis gases in a wind tunnel and in prescribed burns. Int J Wildland Fire 2023;32:56–77. https://doi.org/10.1071/WF22079.
[122] White FM. Heat and mass transfer. Reading, Mass: Addison-Wesley; 1988.